

Learning from Incremental Directional Corrections

Wanxin Jin
wanxinjin@gmail.com

Todd D. Murphey
t-murphey@northwestern.edu

Shaoshuai Mou
mous@purdue.edu

Abstract—This paper proposes a technique which enables a robot to learn a control objective function incrementally from human user’s corrections. The human’s corrections can be as simple as directional corrections—corrections that indicate the direction of a control change without indicating its magnitude—applied at some time instances during the robot’s motion. We only assume that each of the human’s corrections, regardless of its magnitude, points in a direction that improves the robot’s current motion relative to an implicit objective function. The proposed method uses the direction of a correction to update the estimate of the objective function based on a cutting plane technique. We establish the theoretical results to show that this process of incremental correction and update guarantees convergence of the learned objective function to the implicit one. The method is validated by both simulations and two human-robot games, where human players teach a 2-link robot arm and a 6-DoF quadrotor system for motion planning in environments with obstacles.

I. INTRODUCTION

For tasks where robots work in proximity to human users, a robot is required to not only guarantee the accomplishment of a task but also complete it in a way that a human user prefers. Different users may have difference preferences about how the robot should perform the task. Such customized requirements usually lead to considerable workload of robot programming, which requires human users to have expertise to design and repeatedly tune robot’s controllers until achieving satisfactory robot behaviors.

To circumvent the expertise requirement in traditional robot programming, learning from demonstrations (LfD) empowers a non-expert human user to program a robot by only providing demonstrations. In existing LfD techniques [1], a human user first provides a robot with behavioral demonstrations in a *one-time* manner, then the robot learns a control policy or a control objective function *off-line* from the demonstrations. Successful examples include autonomous driving [2], robot manipulation [3], and motion planning [4]. In some practical cases, the *one-time and offline nature* of LfD can introduce challenges. For example, when the demonstrations are insufficient to infer the objective function due to low data informativeness [5] or significant deviation from the optimal data [6], new demonstrations have to be re-collected and the robot has to be re-trained. Importantly, acquiring an optimal demonstration in a one-shot fashion for the systems of high degree-of-freedoms can be challenging [6], because the human demonstrator has to move the robot in all degrees-of-freedom in a spatially and temporally consistent manner.

In this work, we address the above challenges by developing a new programming scheme that enables a non-expert human user to program a robot by *incrementally improving* the robot’s motion. For instance, consider the example of a robot that plans motion under a (random) control objective function.

While it is executing the motion, a human user who supervises the robot will find the robot’s motion is not satisfactory; thus, the human user applies a correction to the robot during its motion execution. Then, the robot uses the correction to update its control objective function. This process of planning-correction-update repeats until the robot eventually achieves a control objective function such that its resulting trajectory agrees with the human user’s expectation. In this learning procedure, the human’s each correction does not necessarily move the robot to the optimal motion, but merely an *incremental improvement* of the robot’s current motion towards the human’s expectation, thus reducing the workload of a non-expert user when programming a robot compared to LfD. In addition to the incremental learning capability, the proposed learning from directional corrections technique in this work also has the following highlights.

1) The proposed method only requires human’s *directional corrections*. A directional correction is a correction that only contains directional information and does not necessarily need to be magnitude-specific. For instance, for teaching a mobile robot, the directional corrections are simply as ‘left’ or ‘right’ without dictating how far the robot should move.

2) The human’s directional corrections to the robot’s motion can be *sparse*. That means that the corrections can be applied only at *sparse time instances* within the time horizon of the robot’s motion. The learning is performed directly based on the sparse corrections, without attaining/retaining any intermediate corrected trajectory that may introduce inaccuracy.

3) Both theoretical results and experiments are established to show the convergence of the proposed learning algorithm. Specifically, we validate the method on two human-robot games and the results show that the proposed method enables a robot to efficiently learn a control objective function for the desired motion with few human’s directional corrections.

A. Related Work

1) *Offline Learning from Demonstrations*: To learn a control objective function from demonstrations, the available approaches include inverse optimal control [7]–[9] and inverse reinforcement learning [10]–[12], where given optimal demonstrations, an objective function that explains such demonstrations is inferred and used for motion control and planning. Despite the significant progress achieved in theory and applications [2], [3], [13]–[15], LfD approaches could be inconvenient in some practical situations. First, demonstrations in LfD are usually given in a *one-time* manner and the learning process is usually performed *offline* after the demonstrations are obtained. In the case when the given demonstration data is insufficient to learn the objective function from, such as low

data informativeness as discussed in [5], or the demonstrations significantly deviates from the optimal ones, the data has to be re-collected and the whole learning process has to be re-run. Second, existing LfD techniques [8]–[12] normally assume optimality of the demonstration data, which is challenging to obtain for robots with high degree-of-freedoms. For example, when producing demonstrations for a humanoid robot, a human demonstrator has to account for the motion in all degrees in a spatially and temporally consistent manner. [6].

2) *Online Learning from Feedback or Physical Corrections*: Compared to offline LfD, learning from corrections or feedback enables a human user to incrementally correct the robot's current motion, making it more accessible for the non-expert users who cannot provide optimal demonstrations in a one-time manner [16]. The key assumption for learning from corrections or feedback is that the corrected robot's motion is better than that before the correction. Under this assumption, [6] proposes a co-active learning method, in which a robot receives human's feedback to update its objective function. The human's feedback includes the passive selection of a top-ranked robot trajectory or the active physical interference for providing a preferred robot trajectory. By defining a learning regret, which quantifies the *average* misalignment of the score values between the human's intended trajectory and robot's trajectory under the human's *implicit* objective function, the authors show the convergence of the regret. But since the regret is an average indicator over the entire learning process, one still cannot explicitly tell if the learned objective function is actually converging towards the human's implicit one.

Very recently, the authors in [17]–[19] approach learning from corrections from the perspective of a partially observable Markov decision process (POMDP), where human's corrections are viewed as the observations about the unknown objective function parameters. By approximating the observation model and applying maximum a posteriori estimation, they obtain a learning update that is similar to the co-active learning [6]. To handle the sparse corrections that a human user applies only at sparse time instances during the robot's motion, these methods apply the trajectory deformation technique [20] to interpret each single-time-step correction through a human indented trajectory, i.e., a deformed robot trajectory. Although achieving promising results, choosing the hyper-parameters in the trajectory deformation is challenging, which can affect the learning performance [18]. In addition, these methods have not provided any convergence guarantee of the learning process.

Both the above co-active learning and POMDP-based learning require a dedicated setup or process to obtain the *human indented/feedback trajectories*. Specifically, in co-active learning, a robot is switched to the screening and zero-force gravity-compensation modes to obtain a human feedback trajectory, and in the POMDP-based method, the human intended trajectory is obtained by deforming the robot's current trajectory based on a correction using trajectory deformation method. These intermediate steps may introduce inaccurate artificial aspects to the learning process, which could lead to failure of the approach. For example, when a user physically corrects a robot, the magnitude of a correction, i.e., how much the correction should be, can be difficult to determine. If not

chosen properly, the given correction may be overshot, i.e., too much correction. Such a overshooting correction can make the obtained human feedback trajectory violate the assumption of improving the robot's motion. In fact, as we will demonstrate in Sections II and V-C, the more closer the robot is approaching to the expected trajectory, the more difficult the choice of a proper correction magnitude will be, which can lead to learning inefficiency. Also, for POMDP-based methods, when one applies the trajectory deformation, the choice of hyper-parameters will determine the shape of the human intended trajectory and thus finally affect the learning performance, as discussed in [18].

B. Contributions

This paper develops a new method to learn a robot objective function incrementally from human's directional corrections. Compared to the existing methods above, the distinctions and contributions of the proposed method are stated as follows.

- 1) The proposed method learns a robot control objective function only using the *direction information* of human's corrections. It only requires that a correction, regardless of magnitude, has a direction of incrementally improving robot's current motion. As we will later show in Sections II and V-C, the feasible corrections that satisfy such a requirement always account for half of the entire input space, making it more flexible for a human user to choose corrections from.
- 2) Unlike existing learning techniques which usually require an intermediate setup/process to obtain a human indented trajectory, the proposed method learns a control objective function *directly from directional corrections*. The directional corrections can be *sparse*, i.e., the corrections only applied at some time instances within the time horizon of robot's motion.
- 3) The proposed learning algorithm is developed based on the cutting plane technique, which has a straightforward intuitive geometric interpretation. We have established the theoretical results to show the convergence of the learned objective function to the human's implicit one.

The proposed method is validated by two human-robot games based on a two-link robot arm and a 6-DoF quadrotor maneuvering system, where a human player, by applying directional corrections, teaches the robot for motion control in environments with obstacles. The experiment results demonstrate that the proposed method enables a non-expert human player to train a robot to learn an effective control objective function for desired motion with few directional corrections.

In the following, Section II describes the problem. Section III proposes the main algorithm outline. Section IV provides theoretical results of the algorithm and its detailed implementation. Numerical simulations and comparison are in Section V. Section VI presents the experiments on two human-robot games. Conclusions are drawn in Section VIII.

II. PROBLEM FORMULATION

Consider a robot with the following dynamics:

$$\mathbf{x}_{t+1} = \mathbf{f}(\mathbf{x}_t, \mathbf{u}_t), \quad \text{with } \mathbf{x}_0, \quad (1)$$

where $\mathbf{x}_t \in \mathbb{R}^n$ is the robot state, $\mathbf{u}_t \in \mathbb{R}^m$ is the control input, $\mathbf{f} : \mathbb{R}^n \times \mathbb{R}^m \mapsto \mathbb{R}^n$ is differentiable, and $t = 1, 2, \dots$ is the time step. As commonly used by objective learning methods such as [5], [6], [9]–[12], [16]–[19], we suppose that the robot control cost function obeys the following parameterized form

$$J(\mathbf{u}_{0:T}, \theta) = \sum_{t=0}^T \theta' \phi(\mathbf{x}_t, \mathbf{u}_t) + h(\mathbf{x}_{T+1}), \quad (2)$$

where $\phi : \mathbb{R}^n \times \mathbb{R}^m \mapsto \mathbb{R}^r$ is a vector of the *specified* features (or basis functions) for the running cost; $\theta \in \mathbb{R}^r$ is a vector of weights, which are *tunable*; and $h(\mathbf{x}_{T+1})$ is the final cost that penalizes the final state \mathbf{x}_{T+1} . For a given choice of θ , the robot chooses a sequence of inputs $\mathbf{u}_{0:T}$ over the time horizon T by optimizing (2) subject to (1), producing a trajectory

$$\xi_\theta = \{\mathbf{x}_{0:T+1}^\theta, \mathbf{u}_{0:T}^\theta\}. \quad (3)$$

For the purpose of readability, we occasionally write the cost function (2) as $J(\theta)$.

For a specific task, suppose that a human's expectation of the robot's trajectory corresponds to an *implicit* cost function $J(\theta^*)$ in the same form of (2) with θ^* . Here, we call θ^* the *expected weight vector*. In general cases, a human user may neither explicitly write down the value of θ^* nor demonstrate the corresponding optimal trajectory ξ_{θ^*} to the robot, but the human user can tell whether the robot's current trajectory is *satisfactory* or not. A trajectory of the robot is satisfactory if it minimizes $J(\theta^*)$; otherwise, it is not satisfactory. In order for the robot to achieve $J(\theta^*)$ (and thus generates a satisfactory trajectory), the human user is only able to make corrections to the robot during its motion, based on which the robot updates its guess of θ towards θ^* .

The process for a robot to learn from human's corrections in this paper is iterative. Each iteration basically includes three steps: planning, correction and update. Let $k = 1, 2, 3, \dots$, denote the iteration index and let θ_k denote the robot's weight vector guess at iteration k . At $k = 1$, the robot is initialized with an arbitrary weight vector guess θ_1 . At iteration $k = 1, 2, 3, \dots$, the robot first performs trajectory *planning*, i.e. achieves ξ_{θ_k} by minimizing the cost function $J(\theta_k)$ in (2) subject to its dynamics (1). During robot's execution of ξ_{θ_k} , the human user gives a *correction* denoted by $\mathbf{a}_{t_k} \in \mathbb{R}^m$ to the robot in its input space. Here, $t_k \in \{0, 1, \dots, T\}$, called *correction time*, indicates at which time step within the horizon T the correction is made. After receiving \mathbf{a}_{t_k} , the robot then performs *update*, i.e. change its guess θ_k to θ_{k+1} according to an update rule to be developed later.

Each human's correction \mathbf{a}_{t_k} is assumed to satisfy the following condition:

$$\langle -\nabla J(\mathbf{u}_{0:T}^{\theta_k}, \theta^*), \bar{\mathbf{a}}_k \rangle > 0, \quad k = 1, 2, 3, \dots. \quad (4)$$

Here

$$\bar{\mathbf{a}}_k = [\mathbf{0}' \quad \dots \quad \mathbf{a}'_{t_k} \quad \dots \quad \mathbf{0}']' \in \mathbb{R}^{m(T+1)}, \quad (5)$$

with \mathbf{a}_{t_k} being the t_k -th entry and $\mathbf{0} \in \mathbb{R}^m$ else; $\langle \cdot, \cdot \rangle$ is the dot product; and $-\nabla J(\mathbf{u}_{0:T}^{\theta_k}, \theta^*)$ is the gradient-descent of $J(\theta^*)$ with respect to $\mathbf{u}_{0:T}$ evaluated at robot's current $\xi_{\theta_k} = \{\mathbf{x}_{0:T+1}^{\theta_k}, \mathbf{u}_{0:T}^{\theta_k}\}$. Note that the condition in (4) does not require a specific value to the magnitude of \mathbf{a}_{t_k} but requires

its direction roughly around the gradient-descent direction of $J(\theta^*)$. Such correction aims to guide the robot's trajectory ξ_{θ_k} towards reducing its cost under $J(\theta^*)$ unless the trajectory is satisfactory. Thus, we call \mathbf{a}_{t_k} satisfying (4) the *incremental directional correction*.

The **problem of interest** in this paper is to develop a rule to update the robot's weight vector guess θ_k to θ_{k+1} such that θ_k converges to θ^* as $k = 1, 2, 3, \dots$, with the human's directional corrections \mathbf{a}_{t_k} under the assumption (4).

Remark. We assume that human user's corrections $\mathbf{a}_{t_k} \in \mathbb{R}^m$ are in the robot's input space, which means that \mathbf{a}_{t_k} can be directly added to the robot's input \mathbf{u}_{t_k} . This can be satisfied in some cases such as autonomous driving, where a user directly manipulates the steering angle of a vehicle. For other cases where the corrections are not readily in the robot's input space, this requirement could be fulfilled through certain human-robot interfaces, which translate the correction signals into the input space. Then, \mathbf{a}_{t_k} denotes the translated correction. The reason why we do not consider the corrections in the robot's state space is that 1) the input corrections may be easier in implementation, and 2) the corrections in the state space can be infeasible for some under-actuated robot systems [21].

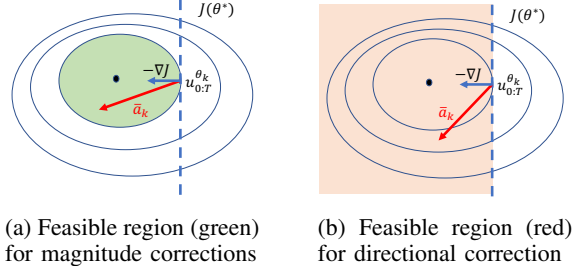


Fig. 1: Magnitude corrections v.s. directional corrections. The contour lines and the optimal/satisfactory trajectory (black dot) of the human's implicit cost function $J(\theta^*)$ are plotted. (a): the green region (a sub-level set) shows all feasible magnitude corrections $\bar{\mathbf{a}}_k$ that satisfy $J(\mathbf{u}_{0:T}^{\theta_k} + \bar{\mathbf{a}}_k, \theta^*) < J(\mathbf{u}_{0:T}^{\theta_k}, \theta^*)$. (b): the orange region (half of the input space) shows all feasible directional corrections $\bar{\mathbf{a}}_k$ that satisfy $\langle -\nabla J(\mathbf{u}_{0:T}^{\theta_k}, \theta^*), \bar{\mathbf{a}}_k \rangle > 0$.

Remark. The assumption in (4) on human's correction \mathbf{a}_{t_k} is less restrictive than the one in [6], [17]–[19], which requires the cost of the corrected robot's trajectory $\mathbf{u}_{0:T}^{\theta_k} + \bar{\mathbf{a}}_k$ is lower than that of original $\mathbf{u}_{0:T}^{\theta_k}$, i.e., $J(\mathbf{u}_{0:T}^{\theta_k} + \bar{\mathbf{a}}_k, \theta^*) < J(\mathbf{u}_{0:T}^{\theta_k}, \theta^*)$. As shown in Fig. 1, this requirement usually leads to constraints in corrections' magnitudes. This is because to guarantee $J(\mathbf{u}_{0:T}^{\theta_k} + \bar{\mathbf{a}}_k, \theta^*) < J(\mathbf{u}_{0:T}^{\theta_k}, \theta^*)$, $\|\bar{\mathbf{a}}_k\|$ has to be chosen from the $J(\mathbf{u}_{0:T}^{\theta_k}, \theta^*)$ -sublevel set of $J(\theta^*)$, as marked by the green region. Furthermore, this region will shrink as it gets close to the optimal trajectory (in black dot), thus making $\|\bar{\mathbf{a}}_k\|$ more difficult to choose when the robot's trajectory is near satisfactory one. In contrast, the directional corrections satisfying (4) always account for half of the entire input space. A human can choose any correction as long as its direction lies in the half space with gradient-descent of $J(\theta^*)$. Thus, (4) is more likely to be satisfied especially for non-expert users.

III. ALGORITHM OUTLINE AND GEOMETRIC INTERPRETATION

In this section, we will present the outline of the proposed main algorithm for a robot to learn from human's incremental directional corrections and then provide a geometric interpretation of the main algorithm. First, we present further analysis on the directional corrections.

A. Equivalent Conditions for Directional Corrections

Before developing the learning procedure, we will show that the assumption in (4) is equivalent to a linear inequality posed on the unknown expected weight vector θ^* , as stated in the following lemma.

Lemma 1. Suppose that the robot's current weight vector guess is θ_k , and its motion trajectory $\xi_{\theta_k} = \{x_{0:T+1}^{\theta_k}, u_{0:T}^{\theta_k}\}$ is a result of minimizing the cost function $J(\theta_k)$ in (2) subject to dynamics in (1). For ξ_{θ_k} , given a human's incremental directional correction a_{t_k} satisfying (4), one has the following inequality equation:

$$\langle h_k, \theta^* \rangle + b_k < 0, \quad k = 1, 2, 3, \dots, \quad (6)$$

with

$$h_k = H'_1(x_{0:T+1}^{\theta_k}, u_{0:T}^{\theta_k}) \bar{a}_k \in \mathbb{R}^r, \quad (7a)$$

$$b_k = \bar{a}'_k H_2(x_{0:T+1}^{\theta_k}, u_{0:T}^{\theta_k}) \nabla h(x_{T+1}^{\theta_k}) \in \mathbb{R}. \quad (7b)$$

Here, \bar{a}_k is defined in (5); $\nabla h(x_{T+1}^{\theta_k})$ is the gradient of the final cost $h(x_{T+1})$ in (2) evaluated at $x_{T+1}^{\theta_k}$; $H_1(x_{0:T+1}^{\theta_k}, u_{0:T}^{\theta_k})$ and $H_2(x_{0:T+1}^{\theta_k}, u_{0:T}^{\theta_k})$ are the coefficient matrices defined as follows:

$$H_1(x_{0:T+1}^{\theta_k}, u_{0:T}^{\theta_k}) = \begin{bmatrix} F_u F_x^{-1} \Phi_x + \Phi_u \\ \frac{\partial f'}{\partial u_T^{\theta_k}} \end{bmatrix} \in \mathbb{R}^{m(T+1) \times r}, \quad (8a)$$

$$H_2(x_{0:T+1}^{\theta_k}, u_{0:T}^{\theta_k}) = \begin{bmatrix} F_u F_x^{-1} V \\ \frac{\partial f'}{\partial u_T^{\theta_k}} \end{bmatrix} \in \mathbb{R}^{m(T+1) \times n}, \quad (8b)$$

with

$$F_x = \begin{bmatrix} I & \frac{-\partial f'}{\partial x_1^{\theta_k}} & \dots & 0 & 0 \\ 0 & I & \dots & 0 & 0 \\ \vdots & \vdots & \ddots & \vdots & \vdots \\ 0 & 0 & \dots & I & \frac{-\partial f'}{\partial x_{T+1}^{\theta_k}} \\ 0 & 0 & \dots & & I \end{bmatrix}, \quad \Phi_x = \begin{bmatrix} \frac{\partial \phi'}{\partial x_1^{\theta_k}} \\ \frac{\partial \phi'}{\partial x_2^{\theta_k}} \\ \vdots \\ \frac{\partial \phi'}{\partial x_T^{\theta_k}} \end{bmatrix}, \quad (9a)$$

$$F_u = \begin{bmatrix} \frac{\partial f'}{\partial u_0^{\theta_k}} & 0 & \dots & 0 \\ 0 & \frac{\partial f'}{\partial u_1^{\theta_k}} & \dots & 0 \\ \vdots & \vdots & \ddots & \vdots \\ 0 & 0 & \dots & \frac{\partial f'}{\partial u_{T+1}^{\theta_k}} \end{bmatrix}, \quad \Phi_u = \begin{bmatrix} \frac{\partial \phi'}{\partial u_0^{\theta_k}} \\ \frac{\partial \phi'}{\partial u_1^{\theta_k}} \\ \vdots \\ \frac{\partial \phi'}{\partial u_{T+1}^{\theta_k}} \end{bmatrix}, \quad (9b)$$

$$V = \begin{bmatrix} 0 & 0 & \dots & 0 & \frac{\partial f}{\partial u_T^{\theta_k}} \end{bmatrix}'. \quad (9c)$$

In above, the dimensions of the matrices are $F_x \in \mathbb{R}^{nT \times nT}$, $F_u \in \mathbb{R}^{mT \times nT}$, $\Phi_x \in \mathbb{R}^{nT \times r}$, $\Phi_u \in \mathbb{R}^{mT \times r}$, $V \in \mathbb{R}^{nT \times n}$. For a general differentiable function $g(x)$ and a specific x^* , $\frac{\partial g}{\partial x^*}$ denotes the Jacobian matrix of $g(x)$ evaluated at x^* .

A proof of Lemma 1 is presented in Appendix A. In Lemma 1, h_k and b_k in (7) are known and depend on both human's correction a_{t_k} and robot's motion trajectory $\xi_{\theta_k} = \{x_{0:T+1}^{\theta_k}, u_{0:T}^{\theta_k}\}$. The above Lemma 1 states that each incremental directional correction a_{t_k} can be equivalently converted to an inequality constraint on the unknown θ^* .

Remark. $H_1(x_{0:T+1}^{\theta_k}, u_{0:T}^{\theta_k})$ and $H_2(x_{0:T+1}^{\theta_k}, u_{0:T}^{\theta_k})$ in Lemma 1 also appear in [5], in which they are shown to be efficiently computed iteratively based on $(x_t^{\theta_k}, u_t^{\theta_k})$, $t = 0, 1, \dots, T$. Specifically, Define and initialize

$$\begin{aligned} H_1(x_{0:1}^{\theta_k}, u_{0:1}^{\theta_k}) &= \frac{\partial f'}{\partial u_0^{\theta_k}} \frac{\partial \phi'}{\partial x_1^{\theta_k}} + \frac{\partial \phi'}{\partial u_0^{\theta_k}}, \\ H_2(x_{0:1}^{\theta_k}, u_{0:1}^{\theta_k}) &= \frac{\partial f'}{\partial u_0^{\theta_k}} \frac{\partial f'}{\partial x_1^{\theta_k}}, \end{aligned} \quad (10a)$$

Perform the iteration with each next state-input $(x_{t+1}^{\theta_k}, u_{t+1}^{\theta_k})$ until $t = T - 1$

$$\begin{aligned} H_1(x_{0:t+1}^{\theta_k}, u_{0:t+1}^{\theta_k}) &= \begin{bmatrix} H_1(x_{0:t}^{\theta_k}, u_{0:t}^{\theta_k}) + H_2(x_{0:t}^{\theta_k}, u_{1:t}^{\theta_k}) \frac{\partial \phi'}{\partial x_{t+1}^{\theta_k}} \\ \frac{\partial f'}{\partial u_t^{\theta_k}} \frac{\partial \phi'}{\partial x_{t+1}^{\theta_k}} + \frac{\partial \phi'}{\partial u_t^{\theta_k}} \end{bmatrix}, \\ H_2(x_{0:t+1}^{\theta_k}, u_{0:t+1}^{\theta_k}) &= \begin{bmatrix} H_2(x_{0:t}^{\theta_k}, u_{0:t}^{\theta_k}) \frac{\partial \phi'}{\partial x_{t+1}^{\theta_k}} \\ \frac{\partial f'}{\partial u_t^{\theta_k}} \frac{\partial f'}{\partial x_{t+1}^{\theta_k}} \end{bmatrix}, \end{aligned} \quad (10b)$$

Finally for $t = T$,

$$\begin{aligned} H_1(x_{0:T+1}^{\theta_k}, u_{0:T}^{\theta_k}) &= \begin{bmatrix} H_1(x_{0:T}^{\theta_k}, u_{0:T-1}^{\theta_k}) \\ \frac{\partial \phi'}{\partial u_T^{\theta_k}} \end{bmatrix}, \\ H_2(x_{0:T+1}^{\theta_k}, u_{0:T}^{\theta_k}) &= \begin{bmatrix} H_2(x_{0:T}^{\theta_k}, u_{0:T-1}^{\theta_k}) \\ \frac{\partial f'}{\partial u_T^{\theta_k}} \end{bmatrix}. \end{aligned} \quad (10c)$$

The above iterative property facilitates the computation of H_1 and H_2 by avoiding the inverse of the large matrix F_x in (8), significantly reducing computational cost in solving for (8).

B. Outline of the Main Algorithm

In order to achieve θ^* , at each iteration k , we let $\Omega_k \subseteq \Theta$ denote a weight search space such that $\theta^* \in \Omega_k$ and $\theta_k \in \Omega_k$ for all $k = 1, 2, 3, \dots$. This Ω_k can be thought of as the possible location of θ^* , and θ_k as a weight vector guess to θ^* . Rather than a rule to guide θ_k towards θ^* , we will develop a rule to update Ω_k to Ω_{k+1} such that a useful scalar measure of the size of Ω_k will converge to 0.

Main Algorithm (Outline): In the proposed main algorithm, we initialize the weight search space Ω_0 to be

$$\Omega_0 = \{\theta \in \mathbb{R}^r \mid -\underline{r}_i \leq [\theta]_i \leq \bar{r}_i, i = 1, \dots, r\}, \quad (11)$$

where \underline{r}_i and \bar{r}_i are non-negative constants denoting the lower bound and upper bound for the i th entry in θ denoted as $[\theta]_i$, respectively. Here, \underline{r}_i and \bar{r}_i can be chosen large enough to include $\theta^* \in \Omega_0$. The learning proceeds with each iteration $k = 1, 2, \dots$, including the following steps:

Step 1: Choose a weight vector guess $\theta_k \in \Omega_{k-1}$ from the weight search space Ω_{k-1} (We will discuss how to choose such $\theta_k \in \Omega_{k-1}$ in Section IV).

Step 2: The robot restarts and plans its motion trajectory ξ_{θ_k} by solving an optimal control problem with the cost function $J(\theta_k)$ and dynamics in (1). While the robot is executing ξ_{θ_k} , a human user applies a directional correction a_{t_k} at time t_k . Then, a hyperplane $\langle h_k, \theta \rangle + b_k = 0$ is obtained by (6)-(7).

Step 3: Update the weight search space Ω_{k-1} to Ω_k :

$$\Omega_k = \Omega_{k-1} \cap \{\theta \in \Theta \mid \langle h_k, \theta \rangle + b_k < 0\}. \quad (12)$$

We provide a few remarks to the above outline of the main algorithm. For initialization in (11), we allow entries of θ to have different lower and upper bounds, which may come from the robot's rough pre-knowledge about the range of each weight. Simply but not necessarily, one could initialize

$$\Omega_0 = \{\theta \in \mathbb{R}^r \mid \|\theta\|_\infty \leq R\}, \quad (13)$$

where

$$R = \max\{r_i, \bar{r}_i, i = 1, \dots, r\}. \quad (14)$$

In Step 1, one chooses $\theta_k \in \Omega_{k-1}$. Soon we will show $\theta^* \in \Omega_k$ for all $k = 1, 2, 3, \dots$. Thus, one will expect θ_k to be closer to θ^* if the main algorithm could make Ω_k smaller. In fact, the weight search space Ω_k is non-increasing because $\Omega_k \subseteq \Omega_{k-1}$ by (12) in Step 3. A careful choice of θ_k to guarantee the strict reduction of a size measure of Ω_k will be given in Section IV. In Step 2, the robot's trajectory planning is performed by solving an optimal control problem with the cost function $J(\theta_k)$ in (2) and the dynamics constraint in (1). This can be done by many trajectory optimization methods such as [22] or existing optimal control solvers such as [23]. With the robot's trajectory ξ_{θ_k} and the human's directional correction a_{t_k} , the hyperplane $\langle h_k, \theta \rangle + b_k = 0$ can be obtained by (6)-(7). The detailed implementation of the main algorithm with the choice of θ_k and termination criterion will be presented in next section.

The proposed main algorithm also leads to the following lemma:

Lemma 2. Under the proposed main algorithm, one has

$$\langle h_k, \theta_k \rangle + b_k = 0, \quad \forall k = 1, 2, 3, \dots \quad (15)$$

and

$$\theta^* \in \Omega_k, \quad \forall k = 1, 2, 3, \dots \quad (16)$$

A proof of Lemma 2 is given in Appendix B. Lemma 2 has intuitive geometric explanations. Note that (15) suggests θ_k is always in the hyperplane $\langle h_k, \theta \rangle + b_k = 0$. Moreover, (16) suggests that although the proposed algorithm directly updates the weight search space Ω_k , the expected weight vector θ^* always lies in Ω_k . Intuitively, the smaller the search space Ω_k is, the closer θ^* is to θ_k .

C. Geometric Interpretation to Updating Ω_k

In this part, we will provide an interpretation of the proposed main algorithm through a geometric perspective. For simplicity of illustrations, we assume $\theta \in \mathbb{R}^2$ in this subsection.

At k th iteration in Fig. 2a, a weight vector guess θ_k (colored in red) is picked from the current weight search space Ω_{k-1}

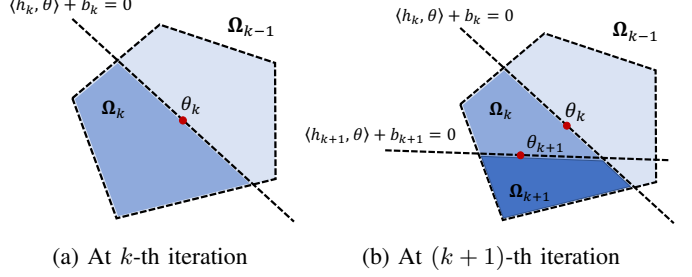


Fig. 2: Illustration of updating Ω_k .

(colored in light blue), i.e., $\theta_k \in \Omega_{k-1}$. By Step 2 in the main algorithm, we obtain a hyperplane $\langle h_k, \theta \rangle + b_k = 0$ (in black dashed line), which cuts through the weight search space Ω_{k-1} into two portions. By (15) in Lemma 2, we know that θ_k also lies on this hyper-plane because $\langle h_k, \theta_k \rangle + b_k = 0$. By Step 3 in the main algorithm, we only keep one of the two cut portions, which is the interaction space between Ω_{k-1} and the half space $\langle h_k, \theta \rangle + b_k < 0$, and the kept portion will be used as the weight search space for the next iteration, that is, $\Omega_k = \Omega_{k-1} \cap \{\theta \mid \langle h_k, \theta \rangle + b_k < 0\}$, as shown in the blue region in Fig. 2a. The above procedure repeats also for iteration $k+1$, as shown in the right panel of Fig. 2b, and finally produces a smaller search space Ω_{k+1} colored in the darkest blue in Fig. 2b. From (12), one has $\Omega_0 \supseteq \dots \supseteq \Omega_{k-1} \supseteq \Omega_k \supseteq \Omega_{k+1} \supseteq \dots$. Moreover, by (16) in Lemma 2, we note that the expected weight vector θ^* is always inside Ω_k whenever k is.

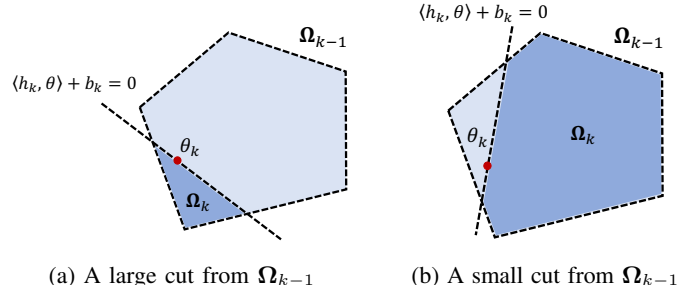


Fig. 3: Illustration of how different directional corrections a_{t_k} affect the reduction of the weight search space Ω_{k-1} .

Besides the above geometric illustration, we also have the following observations:

- (1) The key idea of the proposed main algorithm is to cut and remove the weight search space Ω_{k-1} as each directional correction a_{t_k} is given. Thus, we always expect that Ω_{k-1} can quickly diminish to a very small space as k increases, because thereby we can say that the robot's current guess θ_k is close to the expected weight vector θ^* . As shown in Fig. 2, the reduction rate of Ω_{k-1} depends on two factors: the human's directional correction a_{t_k} , and how to choose $\theta_k \in \Omega_{k-1}$.
- (2) From (7), we note that the human's directional correction a_{t_k} determines h_k , which is the normal vector of hyperplane $\langle h_k, \theta \rangle + b_k = 0$. When fixing the choice of the weight vector guess θ_k , we can think of the hyperplane rotates around θ_k with different choices of a_{t_k} , which

finally results in different removals of Ω_{k-1} , as illustrated in Fig. 3.

- (3) How to choose θ_k from Ω_{k-1} defines the specific position of the hyperplane $\langle h_k, \theta \rangle + b_k = 0$, because the hyperplane is always passing through θ_k by Lemma 2. Thus, θ_k also affects how Ω_{k-1} is cut and removed. This can be illustrated by comparing Fig. 2a with Fig. 3a.

Based on the above discussions, the convergence of the proposed main algorithm is determined by the reduction of the weight search space Ω_{k-1} . This depends on both the human's directional corrections a_{t_k} (hard to be predicted by the robot) and the robot's choice of the weight vector guess $\theta_k \in \Omega_{k-1}$. In the next section, we will present a way for robot to choose θ_k to guarantee the convergence of the proposed algorithm.

IV. ALGORITHM IMPLEMENTATION WITH CONVERGENCE ANALYSIS

In this section, we will specify the choice of θ_k , provide the convergence analysis of the main algorithm, and finally present a detailed implementation of the algorithm with termination criterion.

A. Choice of θ_k

Under the proposed main algorithm, at each iteration k , the weight search space Ω_{k-1} is updated according to (12), i.e.,

$$\Omega_k = \Omega_{k-1} \cap \{\theta \in \Theta \mid \langle h_k, \theta \rangle + b_k < 0\}.$$

In order to evaluate the reduction of the weight search space, it is straightforward to use the volume of the (closure) weight search space Ω_k , denoted as $\text{Vol}(\Omega_k)$, and the zero volume implies the convergence of the search space [24]. By $\Omega_k \subseteq \Omega_{k-1}$ in (12), we know that $\text{Vol}(\Omega_k)$ is non-increasing. In the following we will further develop a way such that $\text{Vol}(\Omega_k)$ is strictly decreasing under the proposed algorithm; i.e., there exists a constant $0 \leq \alpha < 1$ such that

$$\text{Vol}(\Omega_k) \leq \alpha \text{Vol}(\Omega_{k-1}). \quad (17)$$

In order to achieve (17), we note that different choices of $\theta_k \in \Omega_{k-1}$ will lead to different reduction of Ω_{k-1} : as indicated in Fig. 3a, a large volume reduction from Ω_{k-1} to Ω_k is achieved while the choice of θ_k in Fig. 3b leads to a very small volume reduction. This observation motivates us that to avoid a very small volume reduction, one intuitively chooses θ_k at the *center* of the weight search space Ω_{k-1} . Specifically, we use the center of the maximum volume ellipsoid inscribed within the search space as defined below.

Definition 1 (Maximum Volume inscribed Ellipsoid [25]). *Given a compact convex set Ω , the maximum volume ellipsoid (MVE) inscribed within Ω , defined as \mathbf{E} , is represented by*

$$\mathbf{E} = \{\bar{B}\theta + \bar{d} \mid \|\theta\|_2 \leq 1\}. \quad (18)$$

Here, $\bar{B} \in \mathbb{S}_{++}^r$ (i.e., a $r \times r$ positive definite matrix); $\bar{d} \in \mathbb{R}^r$ is called the *center* of \mathbf{E} ; and \bar{B} and \bar{d} solve the optimization:

$$\begin{aligned} \max_{\mathbf{d}, B \in \mathbb{S}_{++}^r} \quad & \log \det B \\ \text{s.t.} \quad & \sup_{\|\theta\|_2 \leq 1} I_\Omega(B\theta + \mathbf{d}) \leq 0, \end{aligned} \quad (19)$$

where $I_\Omega(\theta) = 0$ for $\theta \in \Omega$ and $I_\Omega(\theta) = \infty$ for $\theta \notin \Omega$.

Based on Definition 1, we let \mathbf{E}_k denote the MVE inscribed within Ω_k with \mathbf{d}_k denoting the center of \mathbf{E}_k . For the choice of θ_{k+1} at iteration $k+1$, we choose the weight vector guess

$$\theta_{k+1} = \mathbf{d}_k \quad (20)$$

as illustrated in Fig. 4. Other choices for θ_{k+1} as a center of the search space are discussed in Appendix C.

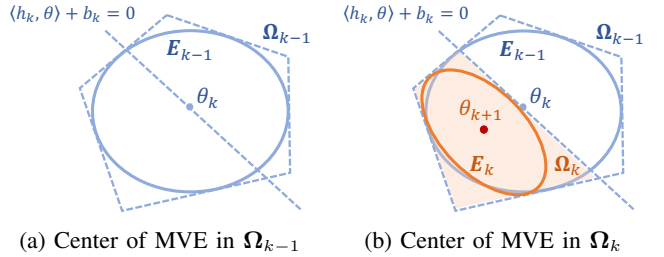


Fig. 4: Illustration of choosing weight vector guess θ_{k+1} as the center of MVE \mathbf{E}_k inscribed in weight search space Ω_k .

We now present a computational method to achieve \mathbf{d}_k , i.e. the center of MVE \mathbf{E}_k inscribe within Ω_k . Recall that in the proposed main algorithm, the initialization of Ω_0 in (11) is

$$\Omega_0 = \{\theta \in \mathbb{R}^r \mid -r_i \leq \theta_i \leq \bar{r}_i, i = 1, \dots, r\},$$

with $[\theta]_i$ the i th entry of θ . This can be equivalently rewritten as a set of linear inequalities:

$$\Omega_0 = \left\{ \theta \mid \begin{array}{l} \langle e_i, \theta \rangle - \bar{r}_i \leq 0, \\ -\langle e_i, \theta \rangle - \underline{r}_i \leq 0, \end{array} i = 1, \dots, r \right\}, \quad (21)$$

where e_i is the unit vector with the i th entry equal to 1. Then, following the update in (12), Ω_k is also a compact polytope, which can be written as

$$\Omega_k = \left\{ \theta \mid \begin{array}{l} \langle e_i, \theta \rangle - \bar{r}_i \leq 0, i = 1, \dots, r; \\ -\langle e_i, \theta \rangle - \underline{r}_i \leq 0, i = 1, \dots, r; \\ \langle h_j, \theta \rangle + b_j < 0, j = 1, \dots, k \end{array} \right\}. \quad (22)$$

As a result, in (19), solving the center \mathbf{d}_k of the MVE \mathbf{E}_k inscribed within Ω_k becomes a convex programming [25], as stated by the following lemma.

Lemma 3. *For a polytope Ω_k in (22), the center \mathbf{d}_k of the MVE \mathbf{E}_k inscribed within Ω_k can be solved by the following convex optimization:*

$$\begin{aligned} \min_{\mathbf{d}, B \in \mathbb{S}_{++}^r} \quad & -\log \det B \\ \text{s.t.} \quad & \|Be_i\|_2 + \langle \mathbf{d}, e_i \rangle \leq \bar{r}_i, i = 1, \dots, r, \\ & \|Be_i\|_2 - \langle \mathbf{d}, e_i \rangle \leq \underline{r}_i, i = 1, \dots, r, \\ & \|\mathbf{Bh}_j\|_2 + \langle \mathbf{d}, \mathbf{h}_j \rangle \leq -b_j, j = 1, \dots, k. \end{aligned} \quad (23)$$

The proof of the above lemma can be found in Chapter 8.4.2 in [25, pp.414]. The above convex optimization can be efficiently solved by existing solver e.g. [26]. In practical implementation of solving (23), since the number of linear inequalities grows as the iteration k increases, which can increase computational cost, the mechanism for dropping some redundant inequalities in (22) can be adopted [24]. Dropping redundant inequalities does not change Ω_k and its volume reduction (convergence). Please see how to identify the redundant inequalities in [24].

B. Exponential Convergence and Termination Criterion

In this part, we will investigate convergence of the volume of Ω_k following the proposed main algorithm and its termination criterion for practical implementation.

Note that the convergence of the proposed algorithm relies on the reduction of $\text{Vol}(\Omega_k)$, which can be guaranteed by the following lemma:

Lemma 4. *Let $\theta_k \in \mathbb{R}^r$ be chosen as the center of the MVE E_{k-1} inscribed within Ω_{k-1} . Then, the update (12) leads to*

$$\frac{\text{Vol}(\Omega_k)}{\text{Vol}(\Omega_{k-1})} \leq (1 - \frac{1}{r}). \quad (24)$$

Lemma 4 is a direct theorem from [27]. Lemma 4 indicates

$$\text{Vol}(\Omega_k) \leq (1 - \frac{1}{r})^k \text{Vol}(\Omega_0).$$

Thus, $\text{Vol}(\Omega_k) \rightarrow 0$ exponentially fast, that is, its convergence speed is as fast as $(1 - \frac{1}{r})^k \rightarrow 0$ as $k \rightarrow \infty$.

In order to implement the main algorithm in practice, we will not only need the exponential convergence as established by Lemma 4, but also a termination criterion, which specifies the maximum number of iterations for a given requirement in terms of $\text{Vol}(\Omega_k)$. Thus we have the following theorem.

Theorem 1. *Suppose Ω_0 is given by (11), and at iteration k , θ_k is chosen as the center d_{k-1} of MVE E_{k-1} inscribed in Ω_{k-1} . Given a termination condition*

$$\text{Vol}(\Omega_k) \leq (2\epsilon)^r$$

with ϵ a user-specified threshold, the main algorithm runs for $k \leq K$ iterations, namely, the algorithm terminates at most K iterations, where

$$K = \frac{r \log(R/\epsilon)}{-\log(1 - 1/r)}, \quad (25)$$

with R given in (14).

Proof. Initially, we have $\text{Vol}(\Omega_0) \leq (2R)^r$. From Lemma 4, after k iterations, we have

$$\text{Vol}(\Omega_k) \leq (1 - \frac{1}{r})^k \text{Vol}(\Omega_0) \leq (1 - \frac{1}{r})^k (2R)^r, \quad (26)$$

which yields to

$$\log \text{Vol}(\Omega_k) \leq k \log(1 - \frac{1}{r}) + \log(2R)^r. \quad (27)$$

When $k = \frac{r \log(R/\epsilon)}{-\log(1 - 1/r)}$,

$$\log \text{Vol}(\Omega_k) \leq -r \log(R/\epsilon) + \log(2R)^r. \quad (28)$$

The above equation is simplified to

$$\log \text{Vol}(\Omega_k) \leq \log(2\epsilon)^r, \quad (29)$$

which means that the termination condition $\text{Vol}(\Omega_k) \leq (2\epsilon)^r$ is satisfied. This completes the proof. ■

On the above Theorem 1 we have the following comments.

Remark. *Since both θ^* and θ_k are always within Ω_k for any $k = 1, 2, 3 \dots$ by Lemma 2, the user-specified threshold ϵ in the termination condition $\text{Vol}(\Omega_k) \leq (2\epsilon)^r$ can be understood*

as an indicator of a distance between the expected weight vector θ^* (usually unknown in practice) and the robot's weight vector guess θ_k . The threshold ϵ is set based on the desired learning accuracy.

C. Implementation of the Main Algorithm

By the termination criterion in Theorem 1 and the choice of θ_k in (20), one could implement the main algorithm in details as presented in Algorithm 1.

Algorithm 1: Learning from incremental directional corrections

Input: Specify a termination threshold ϵ and use it to compute the maximum iteration K by (25).
Initialization: Initial weight search space Ω_0 in (11).
for $k = 1, 2, \dots, K$ **do**
 Choose a weight vector guess $\theta_k \in \Omega_{k-1}$ by Lemma 3;
 Restart and plan a robot trajectory ξ_{θ_k} by solving an optimal control problem with the cost function $J(\theta_k)$ in (2) and the dynamics in (1);
 Robot executes the trajectory ξ_{θ_k} while receiving the human's directional correction a_{t_k} ;
 Compute the coefficient matrices $H_1(x_{0:T+1}^{\theta_k}, u_{0:T}^{\theta_k})$ and $H_2(x_{0:T+1}^{\theta_k}, u_{0:T}^{\theta_k})$ based on (10), and generate the hyperplane and half space $\langle h_k, \theta \rangle + b_k < 0$ by (6)-(7);
 Update the weight search space by
 $\Omega_k = \Omega_{k-1} \cap \{\theta \in \Theta \mid \langle h_k, \theta \rangle + b_k < 0\}$ by (12);
end
Output: θ_K .

V. NUMERICAL EXAMPLES

In this section, we perform numerical simulations on an inverted pendulum and a two-link robot arm to validate the proposed algorithm and provide comparison with related work.

A. Inverted Pendulum

The dynamics of a pendulum is

$$\ddot{\alpha} = \frac{-g}{l} \sin \alpha - \frac{d}{ml^2} \dot{\alpha} + \frac{u}{ml^2}, \quad (30)$$

with α being the angle between the pendulum and the direction of gravity, u is the torque applied to the pivot, $l = 1\text{m}$, $m = 1\text{kg}$, and $d = 0.1$ are the length, mass, and damping ratio of the pendulum, respectively. We discretize the continuous dynamics by the Euler method with a fixed time interval $\Delta = 0.2\text{s}$. The state and control vectors of the pendulum system are defined as $x = [\alpha, \dot{\alpha}]'$ and $u = u$, respectively, and the initial condition is $x_0 = [0, 0]'$. In the cost function (2), we set the weight-feature running cost as

$$\phi = [\alpha^2, \alpha, \dot{\alpha}^2, u^2]' \in \mathbb{R}^4, \quad (31a)$$

$$\theta = [\theta_1, \theta_2, \theta_3, \theta_4]' \in \mathbb{R}^4, \quad (31b)$$

and set the final cost term as $h(x_{T+1}) = 10(\alpha - \pi)^2 + 10\dot{\alpha}^2$, since our goal is to control the pendulum to reach the vertical position. The time horizon is set as $T = 30$.

In numerical examples, we generate “human’s directional corrections” by simulation. Suppose that the expected weight vector is known explicitly: $\boldsymbol{\theta}^* = [0.5, 0.5, 0.5, 0.5]'$. Then, at iteration k , the “human’s” directional corrections \mathbf{a}_{t_k} is generated using the *sign* of the gradient of the true cost function $J(\boldsymbol{\theta}^*)$, that is,

$$\mathbf{a}_{t_k} = -\text{sign} \left(\left[\nabla J(\mathbf{u}_{0:T}^{\boldsymbol{\theta}_k}, \boldsymbol{\theta}^*) \right]_{t_k} \right) \in \mathbb{R}. \quad (32)$$

Here, $\left[\nabla J(\mathbf{u}_{0:T}^{\boldsymbol{\theta}_k}, \boldsymbol{\theta}^*) \right]_{t_k}$ denotes the t_k th entry of ∇J , and the correction time t_k is randomly chosen (evenly distributed) within horizon $[0, T]$. Obviously, the above “human’s directional corrections” satisfies the assumption in (4).

The initial weight search space Ω_0 is set as

$$\Omega_0 = \{\boldsymbol{\theta} \mid 0 \leq [\boldsymbol{\theta}]_i \leq 5, i = 1, 2, 3, 4\}. \quad (33)$$

In Algorithm 1, we set the termination parameter as $\epsilon = 10^{-1}$, and the maximum learning iteration solved by (25) is $K = 55$. We apply Algorithm 1 to learn the expected weight vector $\boldsymbol{\theta}^*$. To illustrate results, we define the guess error $e_{\boldsymbol{\theta}} = \|\boldsymbol{\theta} - \boldsymbol{\theta}^*\|^2$ (i.e., the distance square between the weight vector guess and the expected weight vector $\boldsymbol{\theta}^*$), and plot the guess error $e_{\boldsymbol{\theta}}$ versus the number of iterations k in the top panel of Fig. 5. In the bottom panel of Fig. 5, we plot the directional correction \mathbf{a}_{t_k} applied at each iteration k , where $+1$ and -1 bar denote positive and negative sign (direction) of the correction \mathbf{a}_{t_k} in (32), respectively, and the number inside the bar denotes the correction time t_k that is randomly picked from $\{0, 1, \dots, T\}$.

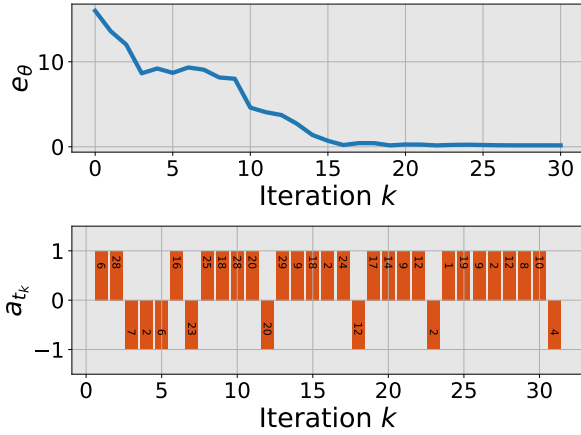


Fig. 5: Learning a pendulum cost function from incremental directional corrections. The upper panel shows the guess error $e_{\boldsymbol{\theta}} = \|\boldsymbol{\theta} - \boldsymbol{\theta}^*\|^2$ versus iteration k , and the bottom panel shows the directional correction \mathbf{a}_{t_k} (i.e., positive or negative) applied at each iteration k , and the value inside each bar is t_k that is randomly picked within the time horizon $[0, 30]$.

Based on the results in Fig. 5, we can see that as the learning iteration k increases, the weight vector guess $\boldsymbol{\theta}_k$ converges to the expected weight vector $\boldsymbol{\theta}^* = [0.5, 0.5, 0.5, 0.5]'$. This shows the validity of the method, as guaranteed by Theorem 1.

B. Two-link Robot Arm System

Here, we test the proposed method on a two-link robot arm. The dynamics of the robot arm system (moving horizontally) is $M(\mathbf{q})\ddot{\mathbf{q}} + C(\mathbf{q}, \dot{\mathbf{q}})\dot{\mathbf{q}} = \boldsymbol{\tau}$, where $M(\mathbf{q})$ is the inertia matrix, $C(\mathbf{q}, \dot{\mathbf{q}})$ is the Coriolis matrix; $\mathbf{q} = [q_1, q_2]'$ is the vector of joint angles, and $\boldsymbol{\tau} = [\tau_1, \tau_2]'$ is the torque vector applied to each joint. The state and control variables for the robot arm control system are defined as $\mathbf{x} = [\mathbf{q}, \dot{\mathbf{q}}]'$ $\in \mathbb{R}^4$ and $\mathbf{u} = \boldsymbol{\tau} \in \mathbb{R}^2$, respectively. The initial condition of the robot arm is set as $\mathbf{x}_0 = [0, 0, 0, 0]'$. All parameters in the dynamics are set as units. We discretize the continuous dynamics using the Euler method with a fixed time interval $\Delta = 0.2$ s. In the cost function (2), we set the weight-feature cost as

$$\boldsymbol{\phi} = [q_1^2, q_1, q_2^2, q_2, \|\mathbf{u}\|^2] \in \mathbb{R}^5, \quad (34a)$$

$$\boldsymbol{\theta} = [\theta_1, \theta_2, \theta_3, \theta_4, \theta_5] \in \mathbb{R}^5, \quad (34b)$$

and set the final cost $h(\mathbf{x}_{T+1}) = 100((q_1 - \frac{\pi}{2})^2 + q_2^2 + \dot{q}_1^2 + \dot{q}_2^2)$, as we aim to control the robot arm to finally reach and stop at the configuration of $\mathbf{q} = [\frac{\pi}{2}, 0]'$. The time horizon is set to be $T = 50$.

We still use simulation to generate “human’s directional corrections”, as similar to the previous experiment. Suppose that we explicitly know the expected weight vector $\boldsymbol{\theta}^* = [1, 1, 1, 1, 1]'$. Then, at each iteration k , the simulation generates a directional correction \mathbf{a}_{t_k} by the sign of the gradient of the true cost function $J(\boldsymbol{\theta}^*)$, that is,

$$\mathbf{a}_{t_k} = -\text{sign} \left(\left[\nabla J(\mathbf{u}_{0:T}^{\boldsymbol{\theta}_k}, \boldsymbol{\theta}^*) \right]_{2t_k:2t_k+1} \right) \in \mathbb{R}^2, \quad (35)$$

where $[\nabla J(\mathbf{u}_{0:T}^{\boldsymbol{\theta}_k}, \boldsymbol{\theta}^*)]_{2t_k:2t_k+1}$ denotes the entries in ∇J at positions from $2t_k$ to $2t_k + 1$ (because the input dimension is $m = 2$), and the correction time t_k is randomly (in an even distribution) chosen from the time horizon $[0, T]$. Note that the sign operator is applied to its augment entry-wise.

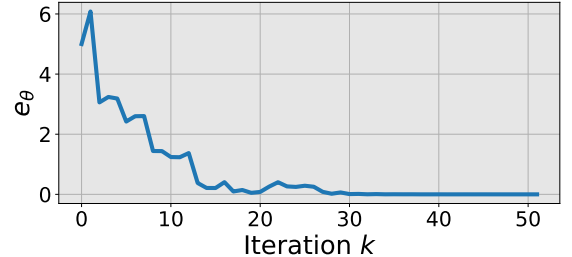


Fig. 6: $e_{\boldsymbol{\theta}} = \|\boldsymbol{\theta} - \boldsymbol{\theta}^*\|^2$ versus iteration k in learning a robot-arm cost function from incremental directional corrections.

The initial weight search space Ω_0 is given by

$$\Omega_0 = \{\boldsymbol{\theta} \mid 0 \leq [\boldsymbol{\theta}]_i \leq 4, i = 1, 2, \dots, 5\}. \quad (36)$$

We set the termination parameter $\epsilon = 10^{-1}$, then the maximum learning iteration is $K = 83$ by (25). We apply Algorithm 1 to learn the expected weight vector $\boldsymbol{\theta}^* = [1, 1, 1, 1, 1]'$. To illustrate results, we define the guess error $e_{\boldsymbol{\theta}} = \|\boldsymbol{\theta} - \boldsymbol{\theta}^*\|^2$ and plot $e_{\boldsymbol{\theta}}$ versus iteration k in Fig. 6. We also plot the directional correction $\mathbf{a}_{t_k} = [a_{t_k,1}, a_{t_k,2}]'$ applied at each iteration k in Fig. 7, where the value inside the bar is the correction time t_k .

Based on the results, we can see that as the iteration increases, the weight vector guess θ_k converges to the expected weight vector θ^* , as guaranteed by Theorem 1. This result again demonstrates the effectiveness of the proposed method.

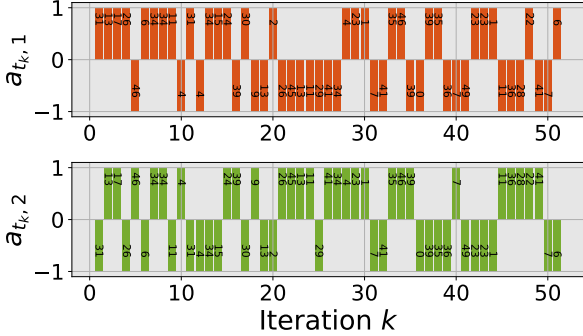


Fig. 7: The directional correction $\mathbf{a}_{t_k} = [a_{t_k,1}, a_{t_k,2}]'$ applied at each iteration k during the learning of the robot-arm cost function. The number inside the bar is the correction time t_k randomly picked within the time horizon $[0, 50]$.

C. Comparison with Related Work

In this part, we compare the proposed method with two related work [6], [17] based on the inverted pendulum system. The dynamics settings and parameters follow the experiment in Section V-A, and the weight-feature cost function is set as (31). According to [17], for each of the human’s corrections, we first utilize the trajectory deformation technique [18] to obtain the corresponding *human intended trajectory*. Specifically, given a correction a_k , the human intended trajectory, denoted as $\bar{\xi}_{\theta_k} = \{\bar{x}_{0:T+1}^{\theta_k}, \bar{u}_{0:T}^{\theta_k}\}$, can be solved by

$$\bar{\mathbf{u}}_{0:T}^{\theta_k} = \mathbf{u}_{0:T}^{\theta_k} + M^{-1} \bar{\mathbf{a}}_k, \quad (37)$$

where $\xi_{\theta_k} = \{x_{0:T+1}^{\theta_k}, u_{0:T}^{\theta_k}\}$ is the robot's current trajectory; M is a matrix that smoothly propagates the local correction augmented vector in (5) along the rest of the trajectory [20]; and $\bar{x}_{0:T+1}^{\theta_k}$ in ξ_{θ_k} is obtained from the robot dynamics in (1) given $\bar{u}_{0:T}^{\theta_k}$. For both [6] and [17], the learning update is

$$\boldsymbol{\theta}_{k+1} = \boldsymbol{\theta}_k + \alpha \left(\boldsymbol{\phi}(\bar{\boldsymbol{\xi}}_{\boldsymbol{\theta}_k}) - \boldsymbol{\phi}(\boldsymbol{\xi}_{\boldsymbol{\theta}_k}) \right), \quad (38)$$

where $\phi(\bar{\xi}_{\theta_k})$ and $\phi(\xi_{\theta_k})$ are the vectors of feature values for the human intended trajectory $\bar{\xi}_{\theta_k}$ and the robot's original trajectory ξ_{θ_k} , respectively. In this comparison experiment, we set M in (37) as the finite differencing matrix [18], and α is 0.0006 (for having best performance). For all methods, the simulated human's corrections are the same, as shown in Fig. 8. To illustrate performance, we still use the guess error $e_{\theta} = \|\theta - \theta^*\|^2$.

We draw the guess error versus iterations for both [6], [17] and the proposed method in Fig. 9. By comparing both results, we can see a clear advantage of the proposed method over [6] [17] in terms of higher learning accuracy. As we have discussed in the related work, the learning update (38) used in [6], [17] only guarantees the convergence of the regret, which is defined as the averaged error of the cost

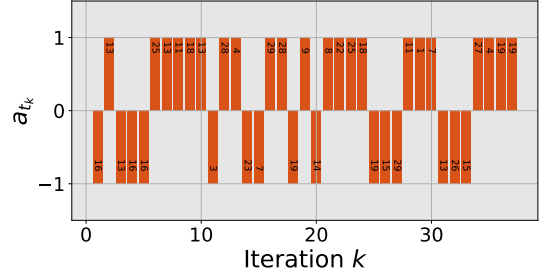


Fig. 8: The correction a_{t_k} at each iteration k . The value labeled inside the bar is the randomly chosen correction time t_k .

values between the human intended trajectory and the robot's trajectory under $J(\theta^*)$ over the entire learning process. Thus, it does not directly lead to the convergence of θ_k towards θ^* , as illustrated in Fig. 9. In contrast, Fig. 9 illustrates that using the proposed approach, the learned cost function quickly converges to $J(\theta^*)$, as guaranteed by Theorem 1.

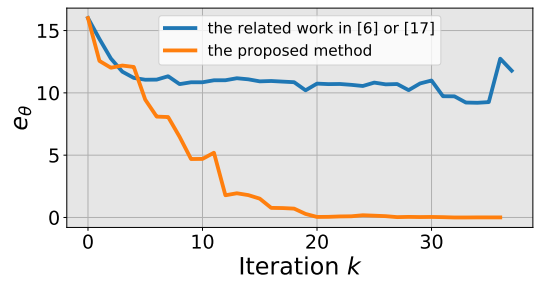


Fig. 9: Comparison between [6], [17] and the proposed method. The figure shows $e_\theta = \|\theta - \theta^*\|^2$ v.s. iteration k .

Throughout the experiment, we find that the methods [6], [17] are not robust against the corrections \mathbf{a}_{t_k} of very larger magnitude. Given a correction \mathbf{a}_{t_k} with a larger magnitude, [6] and [17] are more likely to diverge especially. This is because larger correction magnitude $\|\mathbf{a}_{t_k}\|$ can be overshot (i.e., too large), which thus violates their assumption of improving the robot's motion, i.e., $J(\bar{\mathbf{u}}_{0:T}^{\theta_k}, \theta^*) < J(\mathbf{u}_{0:T}^{\theta_k}, \theta^*)$. We also find that the correction overshooting is more likely to happen at the end of learning process when the robot motion gets close to the optimal one, as we have explained in Section II. This issue has also been illustrated in Fig. 9. At the iteration $k = 35$ in Fig. 9, we see that e_θ instead becomes increased as we use a constant correction magnitude throughout the learning process. In contrast, the proposed method only leverages the direction of \mathbf{a}_{t_k} (negative or positive) regardless of $\|\mathbf{a}_{t_k}\|$; thus there is no overshooting issue with the proposed method. This shows more flexibility of the proposed method than [17] and [6] in terms of choosing proper corrections.

VI. HUMAN-ROBOT GAMES

In this section, we develop two human-robot games, where a real human player online teaches a robot for motion planning through directional corrections. These games are used to validate the effectiveness of the proposed approach in practice. The games are developed on two robot systems/environments:

a two-link robot arm and a 6-DoF quadrotor system, respectively. For each environment, a human player visually inspects robot's motion on a computer screen, meanwhile providing directional corrections through a keyboard. The goal of each game is to train a robot to learn an effective control objective function such that the robot successfully avoids obstacles and reaches a target position.

We have released all codes of the two games for the readers to have hands-on experience with. Please download at <https://github.com/wanxinjin/Learning-from-Directional-Corrections>.

A. Two-link Robot Arm Game

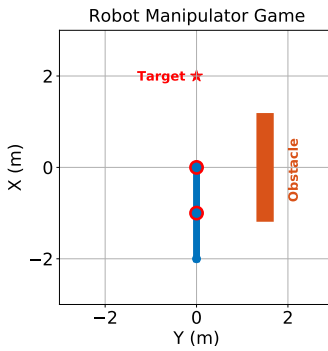


Fig. 10: The robot arm game. The goal is to let a human player teach the robot arm to learn a valid cost function (i.e., the expected weight vector θ^*) by applying incremental directional corrections, such that it successfully moves from the initial condition (current pose) to the target (upward pose) while avoiding the obstacle.

1) *System Setup*: In this game, the dynamics of a two-link robot arm and its parameters follow those in Section V-B. The initial state of the arm is $\mathbf{x} = [-\frac{\pi}{2}, 0, 0, 0]'$, as shown in Fig. 10. For the parameterized cost function $J(\theta)$ in (2), we set the weight-feature running cost as

$$\phi = [q_1^2, q_1, q_2^2, q_2, \|\mathbf{u}\|^2]' \in \mathbb{R}^5, \quad (39a)$$

$$\theta = [\theta_1, \theta_2, \theta_3, \theta_4, \theta_5]' \in \mathbb{R}^5. \quad (39b)$$

Here, the weight-feature cost $\theta' \phi$ is a general second-order polynomial function. It is worth noting that in practice, if one has no prior knowledge/experience about how to choose good features, the general polynomial features are always a good choice. For the final cost $h(\mathbf{x}_{T+1})$ in $J(\theta)$ in (2), we set

$$h(\mathbf{x}_{T+1}) = 100((q_1 - \frac{\pi}{2})^2 + q_2^2 + \dot{q}_1^2 + \dot{q}_2^2), \quad (40)$$

because we aim the robot arm to finally reach and stop at the target vertical pose, i.e., $q_1^{\text{target}} = \frac{\pi}{2}$ and $q_2^{\text{target}} = 0$, as depicted in Fig. 10. It is also worth noting that in practice, the final cost function $h(\mathbf{x}_{T+1})$ in (2) can always be set as the distance to the target state. The time horizon in this robot arm game is set as $T = 50$ (that is, $50\Delta = 10$ s).

Since we choose the polynomial features in (39a), different weight vector θ leads to different robot's trajectories to the target pose. As shown in Fig. 10, we place an obstacle (colored in orange) in the workspace of the robot arm. Without human's

intervention, the robot will move and crash into the obstacle. The goal of the game is to let a human player make directional corrections to the robot arm while it is moving, until the robot arm learns a valid cost function $J(\theta^*)$ (i.e., the expected weight vector θ^*) to successfully avoid the obstacle and reach the target.

2) *Human Correction Interface*: For the above robot arm game, we use keyboards as the interface for a human player to provide directional corrections. We customize the (*up*, *down*, *left*, *right*) keys in a keyboard and associate them with the directional corrections as listed in Table I. During the game, at each iteration, a human player is allowed to press one or multiple keys from (*up*, *down*, *left*, *right*), and the keyboard interface is listening to which key(s) the human player hits and recording the time step of the keystroke(s). The recorded information, i.e., the pressed keys and stroke time, is translated into the directional correction \mathbf{a}_{t_k} in the robot's input space according to Table I. For example, at iteration k , while the robot arm is graphically executing the trajectory ξ_{θ_k} , a human player hits the *up* and *left* keys simultaneously at the time step 10; then the corresponding correction information is translated into $\mathbf{a}_{t_k} = [1, 1]'$ with $t_k = 10$ according to Table I.

TABLE I: Correction interface for the robot arm game.

Keys	Directional correction	Interpretation of correction
<i>up</i>	$\mathbf{a} = [1, 0]$	add counter-close-wise torque to Joint 1
<i>down</i>	$\mathbf{a} = [-1, 0]$	add close-wise torque to Joint 1
<i>left</i>	$\mathbf{a} = [0, 1]$	add counter-close-wise torque to Joint 2
<i>right</i>	$\mathbf{a} = [0, -1]$	add close-wise torque to Joint 2

3) *Game Procedure*: The procedure of this robot arm game is as follows. By default, the robot's initial weight search space Ω_0 is set as

$$\Omega_0 = \{\theta \mid \theta_1, \theta_3 \in [0, 1], \theta_2, \theta_4 \in [-3, 3], \theta_5 \in [0, 0.5]\}. \quad (41)$$

As stipulated by the main algorithm, at each iteration k , the robot arm first chooses a weight vector guess $\theta_k \in \Omega_{k-1}$ by Lemma 3 and then plans the corresponding motion trajectory ξ_{θ_k} (by minimizing the cost function $J(\theta_k)$ subject to the robot's dynamics). While the robot arm is graphically executing the planned trajectory ξ_{θ_k} on the computer screen, a human player inspects the ongoing motion ξ_{θ_k} and provides the directional correction \mathbf{a}_{t_k} via the keyboard interface based on the rules in Table I. Each time the keyboard interface detects the human's player's directional correction \mathbf{a}_{t_k} , the robot arm incorporates such correction \mathbf{a}_{t_k} to update the weight search space from Ω_{k-1} to Ω_k by Step 3 in the main algorithm. This planning-correction-update procedure repeats until the robot arm successfully avoids the obstacle and reaches the target and then the human player will not intervene the robot arm any more—mission accomplished.

4) *Results and Analysis*: We present an illustrative result in Fig. 11, where we show that the robot arm can learn a valid cost function after only four rounds of human's directional corrections (i.e., four iterations). At each iteration k , the robot's current weight vector θ_k and the player's

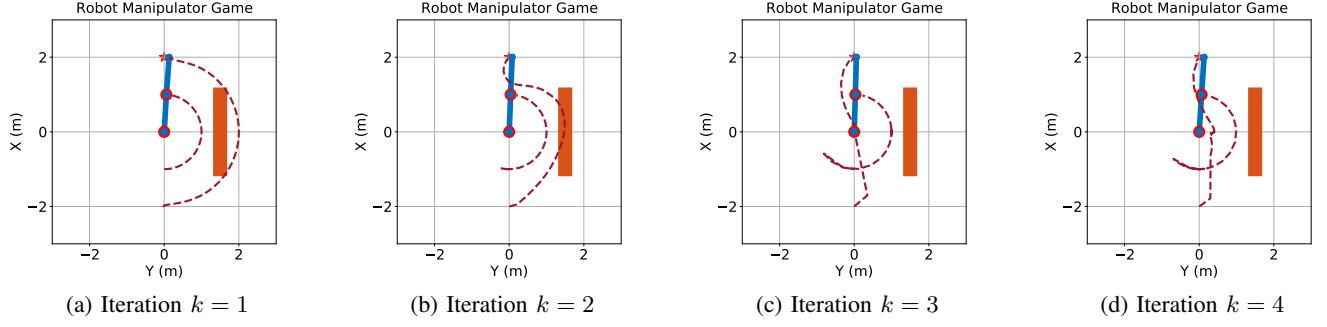


Fig. 11: An illustrative result for the robot arm game. The goal of this game is to let a human player to correct the robot arm while it is acting, until the robot arm learns a valid control objective function (i.e., expected θ^*) for successfully avoiding the obstacle and reaching the target pose. Corresponding to the above sub-figures, the robot's weight vector guess θ_k and the player's directional correction a_k at each iteration k are listed in Table II. In (a), and the robot arm randomly chooses an initial weight vector guess $\theta_1 \in \Omega_0$ and its resulting motion crashes into the obstacle. In (d), the robot arm successfully learns a valid cost function (i.e., the expected θ^*) to avoid the obstacle and reach the target—mission accomplished.

TABLE II: An illustrative result for the robot arm game.

Iteration k	Robot's current weight vector guess θ_k	A human player's directional correction a_{t_k} and correction time t_k
$k = 1$	$\theta_k = [0.50, 0.00, 0.50, -0.00, 0.25]'$	$a_{t_k} = [0, 1]$ (i.e., <i>left</i> key pressed) and $t_k = 11$
$k = 2$	$\theta_k = [0.50, 0.00, 0.50, -1.50, 0.25]'$	$a_{t_k} = [0, 1]$ (i.e., <i>left</i> key pressed) and $t_k = 16$
$k = 3$	$\theta_k = [0.50, 0.00, 0.34, -2.03, 0.25]'$	$a_{t_k} = [-1, 0]$ (i.e., <i>down</i> key pressed) and $t_k = 34$
$k = 4$	$\theta_k = [0.50, 1.48, 0.36, -2.00, 0.25]'$	<i>Mission accomplished!</i> $\theta^* = \theta_k$

correction a_{t_k} are in Table II. From Table II and Fig. 11, we observe that the robot arm has successfully learned an effective cost function to avoid the obstacle and reach the target after four rounds of human's directional corrections. These results indicate that the effectiveness of the proposed method for real human users to train a robot through directional corrections. We also have the following comments.

(i) Throughout the game, we find that the successful teaching of the robot *does not require a human player to have prior experience or much practice with the game*. The result shown in Table II and Fig. 11 is just one of many examples, and a novice player can readily provide another sequence of corrections, such as using different combinations of keys and corrections times, to successfully train the robot arm within few iterations.

(ii) We emphasize that the human's corrections for the robot arm is very intuitive. For example, in Fig. 11a, at first iteration, as we see that the robot arm is crashing into the obstacle, the human correction could be a counter-clock-wise torque applied to joint 2 in order to make the second link bend inward. Thus, we need to press the *left* key according to Table I. For another example, in Fig. 11c, since the first joint is shown moving too fast in counter-clock-wise, the human correction needs to give a clock-wise torque to the first joint in order to make it slow down, and thus the player needs to press the *down* key according to Table I. To gain a better understanding of the method and the game, we encourage the reader to download the game codes and have hand-on experience with the robot arm game.

B. 6-DoF Quadrotor Maneuvering Game

1) *System Setup*: The dynamics of a quadrotor drone flying in $\text{SE}(3)$ (i.e., full position and attitude) space is

$$\dot{\mathbf{r}}_I = \dot{\mathbf{v}}_I, \quad (42a)$$

$$m\dot{\mathbf{v}}_I = m\mathbf{g}_I + \mathbf{f}_I, \quad (42b)$$

$$\dot{\mathbf{q}}_{B/I} = \frac{1}{2}\Omega(\boldsymbol{\omega}_B)\mathbf{q}_{B/I}, \quad (42c)$$

$$J_B \dot{\boldsymbol{\omega}}_B = \boldsymbol{\tau}_B - \boldsymbol{\omega}_B \times J_B \boldsymbol{\omega}_B. \quad (42d)$$

Here, subscripts B and I denote quantities expressed in the quadrotor's body frame and world frame, respectively; m is the mass of the quadrotor; $\mathbf{r}_I \in \mathbb{R}^3$ and $\mathbf{v}_I \in \mathbb{R}^3$ are its position and velocity, respectively; $J_B \in \mathbb{R}^{3 \times 3}$ is its moment of inertia expressed in the body frame; $\boldsymbol{\omega}_B \in \mathbb{R}^3$ is its angular velocity; $\mathbf{q}_{B/I} \in \mathbb{R}^4$ is the unit quaternion [28] describing the attitude of the quadrotor's body frame with respect to the world frame; (42c) is the time derivative of the quaternion with $\Omega(\boldsymbol{\omega}_B)$ the matrix form of $\boldsymbol{\omega}_B$ used for quaternion multiplication [28]; $\boldsymbol{\tau}_B \in \mathbb{R}^3$ is the torque vector applied to the quadrotor; and $\mathbf{f}_I \in \mathbb{R}^3$ is the total force vector applied to the its center of mass (COM). The total force magnitude $\|\mathbf{f}_I\| = f \in \mathbb{R}$ (along the z-axis of the quadrotor's body frame) and the torque $\boldsymbol{\tau}_B = [\tau_x, \tau_y, \tau_z]$ are generated by thrusts $[T_1, T_2, T_3, T_4]$ of the four rotating propellers, which has the following relation

$$\begin{bmatrix} f \\ \tau_x \\ \tau_y \\ \tau_z \end{bmatrix} = \begin{bmatrix} 1 & 1 & 1 & 1 \\ 0 & -l_w/2 & 0 & l_w/2 \\ -l_w/2 & 0 & l_w/2 & 0 \\ c & -c & c & -c \end{bmatrix} \begin{bmatrix} T_1 \\ T_2 \\ T_3 \\ T_4 \end{bmatrix}, \quad (43)$$

with l_w denoting the quadrotor's wing length and c a fixed constant, here $c = 0.1$. In the dynamics, gravity constant $\|\mathbf{g}_I\|$

is set as 10m/s^2 and the other parameters are units. We define the state vector for the quadrotor as

$$\mathbf{x} = [\mathbf{r}_I \ \mathbf{v}_I \ \mathbf{q}_{B/I} \ \boldsymbol{\omega}_B] \in \mathbb{R}^{13}, \quad (44)$$

and define the control input vector as

$$\mathbf{u} = [T_1 \ T_2 \ T_3 \ T_4]' \in \mathbb{R}^4. \quad (45)$$

We discretize the above continuous dynamics of the quadrotor by the Euler method with a fixed time interval $\Delta = 0.1\text{s}$. To achieve $\text{SE}(3)$ control for a quadrotor, we need to carefully design the attitude error. As in [29], we define the attitude error between the quadrotor's attitude \mathbf{q} and a target attitude $\mathbf{q}^{\text{target}}$ as

$$e(\mathbf{q}, \mathbf{q}_{\text{target}}) = \frac{1}{2} \text{trace}(I - R'(\mathbf{q}^{\text{target}})R(\mathbf{q})), \quad (46)$$

where $R(\mathbf{q}) \in \mathbb{R}^{3 \times 3}$ is the direction cosine matrix corresponding to \mathbf{q} (see [28] for more details).

In the cost function in (2), we set the final cost $h(\mathbf{x}_{T+1})$ as

$$h(\mathbf{x}_{T+1}) = \|\mathbf{r}_I - \mathbf{r}_I^{\text{target}}\|^2 + 10\|\mathbf{v}_I\|^2 + 100e(\mathbf{q}_{B/I}, \mathbf{q}_{B/I}^{\text{target}}) + 10\|\mathbf{w}_B\|^2, \quad (47)$$

because we always want the quadrotor to finally land on a target position given by $\mathbf{r}_I^{\text{target}}$ in a target attitude $\mathbf{q}_{B/I}^{\text{target}}$. Here, $\mathbf{r}_I = [r_x, r_y, r_z]'$ is the position of the quadrotor expressed in the world frame. We set the weight-feature cost in (2) as

$$\boldsymbol{\phi} = [r_x^2 \ r_x \ r_y^2 \ r_y \ r_z^2 \ r_z \ \|\mathbf{u}\|^2]' \in \mathbb{R}^7, \quad (48a)$$

$$\boldsymbol{\theta} = [\theta_1 \ \theta_2 \ \theta_3 \ \theta_4 \ \theta_5 \ \theta_6 \ \theta_7]' \in \mathbb{R}^7. \quad (48b)$$

Here, feature vector $\boldsymbol{\phi}$ consists of general polynomial features and different weight vectors $\boldsymbol{\theta} = [\theta_1, \theta_2, \theta_3, \theta_4, \theta_5, \theta_6, \theta_7]'$ will determine how the quadrotor reaches the target (that is, the specific path of the quadrotor). It is again worth noting that in practical situations, if one has no prior knowledge/experience about how to choose good features, general polynomial features are always a good choice, as in (48a).

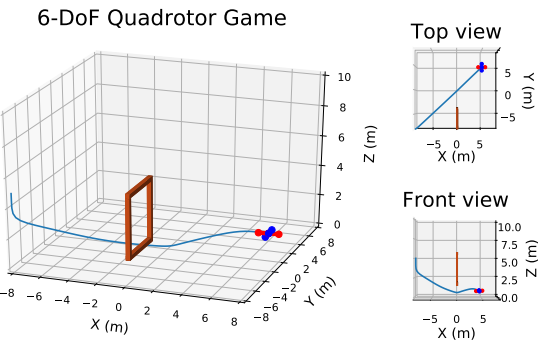


Fig. 12: The 6-DoF quadrotor game. The goal of this game is to let a human player to teach a 6-DoF quadrotor system to learn a valid control cost function (i.e., the expected weight vector $\boldsymbol{\theta}^*$) by providing directional corrections, such that it can successfully fly from the initial position (in bottom left), pass through a gate (colored in brown), and finally land on the specified target (in upper right).

As shown in Fig. 12, the goal of this quadrotor game is to let a human player teach the quadrotor to fly from the initial position $\mathbf{r}_I(0) = [-8, -8, 5]'$ (bottom left), passing through a gate (colored in brown), and finally land on a specified target position $\mathbf{r}_I^{\text{target}} = [8, 8, 0]'$ (upper right) with the target attitude $\mathbf{q}_{B/I}^{\text{target}} = [1, 0, 0, 0]'$. The initial attitude of the quadrotor is $\mathbf{q}_{B/I}(0) = [1, 0, 0, 0]'$ and initial velocity quantities are zeros. The game time horizon is set as $T = 50$, that is, $T\Delta = 5\text{s}$.

2) *Human Correction Interface*: In the 6-DoF quadrotor game, we use keyboards as the interface for a human player to provide directional corrections. Specifically, we use the ('up', 'down', 'w', 's', 'a', 'd') keys and associate them with specific directional correction signals, as listed in Table III. During the game (i.e., algorithm progress), a human player is allowed to press one or multiple combinations of the keys in Table III. The interface is listening to the keystrokes from the human player, and once detected, the keystrokes are translated into the directional corrections according to Table III. Together with the pressed keys, the time step at which a key is hit is also recorded, as the correction time t_k . For example, suppose that while the computer screen is graphically playing the quadrotor executing the trajectory $\xi_{\boldsymbol{\theta}_k}$ (at iteration k), the human player presses 's' key at the time step 5; then, according to Table III, the translated human correction will be $\mathbf{a}_{t_k} = [0, -1, 0, 1]'$ with the correction time $t_k = 5$.

TABLE III: Correction interface for 6-DoF quadrotor game.

Keys	Directional correction	Interpretation of correction
'up'	$T_1=1, T_2=1, T_3=1, T_4=1$	Upward force applied at COM
'down'	$T_1=-1, T_2=-1, T_3=-1, T_4=-1$	Downward force applied at COM
'w'	$T_1=0, T_2=1, T_3=0, T_4=-1$	Negative torque along body-axis x
's'	$T_1=0, T_2=-1, T_3=0, T_4=1$	Positive torque along body-axis x
'a'	$T_1=1, T_2=0, T_3=-1, T_4=0$	Negative torque along body-axis y
'd'	$T_1=-1, T_2=0, T_3=1, T_4=0$	Positive torque along body-axis y

3) *Game Procedure*: The procedure of playing the 6-DoF quadrotor game is as follows. By default, the initial weight research space Ω_0 is set as

$$\Omega_0 = \{\boldsymbol{\theta} \mid \theta_1, \theta_3, \theta_5 \in [0, 1], \theta_2, \theta_4, \theta_6 \in [-8, 8], \theta_7 \in [0, 0.5]\}. \quad (49)$$

As stated by the main algorithm, at each iteration k , the quadrotor chooses a weight vector guess $\boldsymbol{\theta}_k \in \Omega_{k-1}$ by Lemma 3 and plans a motion trajectory $\xi_{\boldsymbol{\theta}_k}$ by minimizing the cost function $J(\boldsymbol{\theta}_k)$ subject to the dynamics constraint in (42). While the quadrotor is graphically executing $\xi_{\boldsymbol{\theta}_k}$ on the computer screen, the keyboard interface is listening to player's directional corrections. Once detecting a player's correction \mathbf{a}_{t_k} , the quadrotor uses such correction to update the weight search space from Ω_{k-1} to Ω_k following Step 3 in the main algorithm. This planning-correction-update procedure repeats until the quadrotor successfully flies through the gate and lands

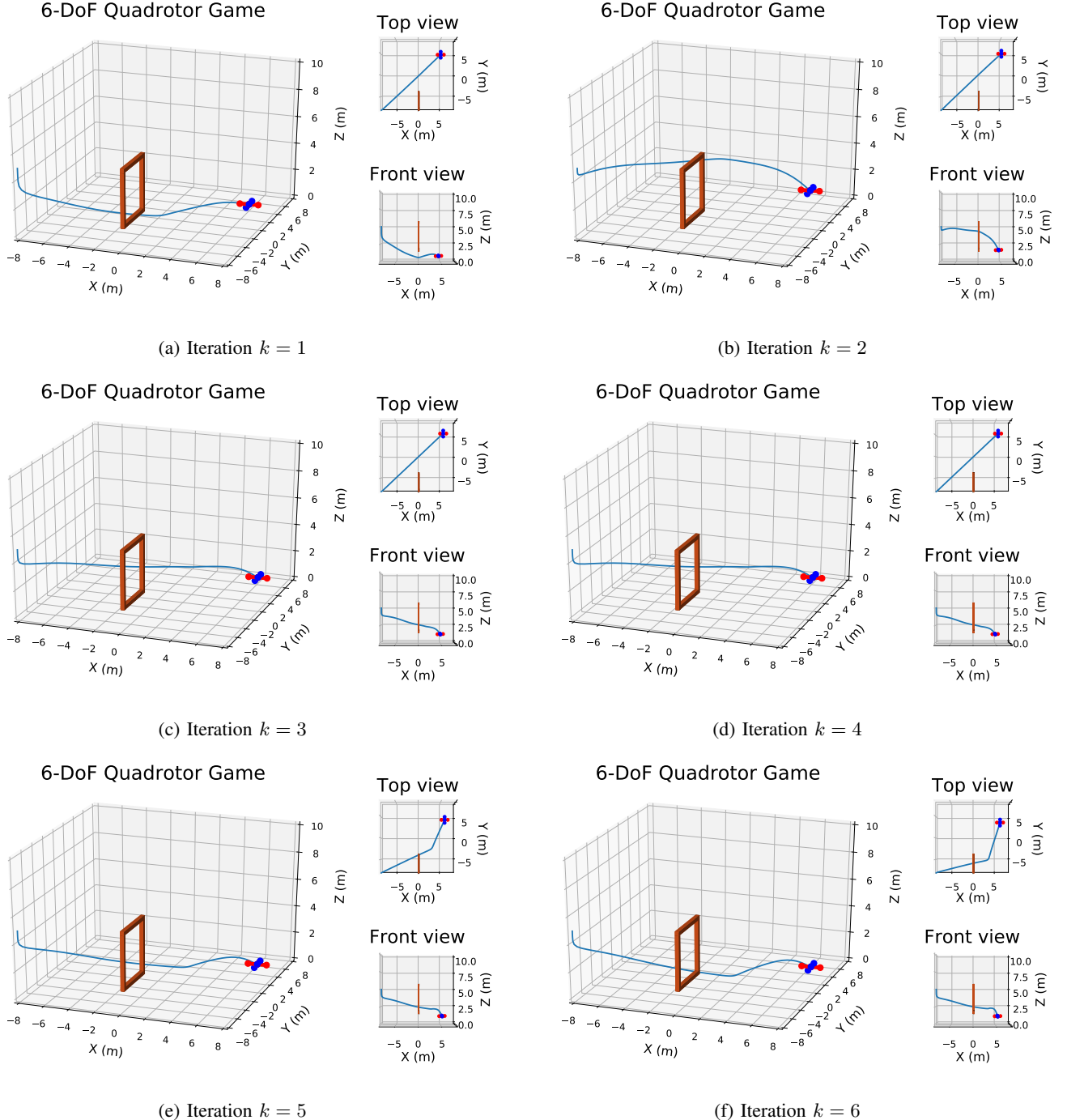


Fig. 13: An illustrative result for the 6-DoF quadrotor game. The goal of this game is to let a human player, through providing directional corrections, to teach a 6-DoF quadrotor to learn a valid control cost function (i.e., expected θ^*) for successfully flying from the initial position, passing through a gate, and finally landing on the target position. Corresponding to each iteration k in the above sub-figures, we also list the robot's current weight vector guess θ_k and the human player's directional correction a_k in Table IV. In (a), at iteration $k = 1$, the quadrotor chooses an initial weight vector guess $\theta_1 \in \Omega_0$. In (c), at iteration $k = 3$, since the human player does not provide any correction, the quadrotor's trajectory at this iteration is the same with the one in (d) (iteration $k = 4$). In (f), at iteration $k = 6$, the quadrotor successfully flies through the gate and lands on the target position, which means that a valid quadrotor cost function is successfully learned—mission accomplished.

TABLE IV: An illustrative result for the 6-DoF quadrotor game.

Iteration k	quadrotor's current weights guess θ_k	A human player's directional corrections \mathbf{a}_{t_k} and correction time steps t_k
$k = 1$	$\theta_k = [0.50, 0.00, 0.50, -0.00, 0.50, -0.00, 0.25]'$	$\mathbf{a}_{t_k} = [1, 1, 1, 1]$ (i.e., up key pressed) and $t_k = 8$ $\mathbf{a}_{t_k} = [1, 1, 1, 1]$ (i.e., up key pressed) and $t_k = 20$
$k = 2$	$\theta_k = [0.50, -0.00, 0.50, -0.00, 0.50, -3.99, 0.25]'$	$\mathbf{a}_{t_k} = [-1, -1, -1, -1]$ (i.e., down key pressed) and $t_k = 14$
$k = 3$	$\theta_k = [0.50, -1.70, 0.50, -1.70, 0.52, -1.89, 0.25]'$	No correction provided (because the human player hesitated)
$k = 4$	$\theta_k = [0.50, -1.70, 0.50, -1.70, 0.52, -1.89, 0.25]'$	$\mathbf{a}_{t_k} = [0, -1, 0, 1]$ (i.e., 's' key pressed) and $t_k = 13$
$k = 5$	$\theta_k = [0.50, -2.76, 0.50, -2.45, 0.60, -2.22, 0.25]'$	$\mathbf{a}_{t_k} = [0, -1, 0, 1]$ (i.e., 's' key pressed) and $t_k = 19$
$k = 6$	$\theta_k = [0.50, -3.11, 0.50, 4.89, 0.65, -2.67, 0.25]'$	Mission accomplished! $\theta^* = \theta_k$

on the target position, and then the human player will not intervene the quadrotor any more—mission accomplished.

4) *Results and Analysis:* We present one illustrative result in Fig. 13 and Table IV. Fig. 13 illustrates the execution of the quadrotor's trajectory ξ_{θ_k} at different iterations k . Table IV presents the weight vector guess θ_k and the human player's correction \mathbf{a}_{t_k} at each iteration k . The results show that within five rounds of directional corrections (i.e., five iterations), the quadrotor is able to learn a valid cost function to successfully fly through the given gate and land on the target landing position. The results again demonstrate the efficiency of the proposed method for a human user to train a robot through directional corrections. Also, we have the following comments.

(i) It is worth mentioning that the successful teaching of the quadrotor in the above game *does not require a human player to have prior experience or much practice with the game*. The above result is just one of the many results, and a new player can choose another sequence of corrections and quickly teach the quadrotor to learn a valid cost function for accomplishing the task.

(ii) The choice of the directional corrections is very intuitive and straightforward. For example, as in Fig. 13a, the quadrotor is flying too low, the player thus has pressed *up* key (Table IV) to let the quadrotor fly higher according to Table III. Also, as in Fig. 13d the quadrotor is flying too left relative to the gate, the player thus have pressed '*s*' key (i.e., a positive torque along the quadrotor's body x-axis) to let the quadrotor tilt right towards the gate. We encourage the reader to have hands-on experience with the above quadrotor game.

VII. CONCLUSION

In this paper, we have proposed an approach which enables a robot to learn an objective function incrementally from human user's directional corrections. The directional corrections, applied by a human user at certain time steps during the robot's motion, can be any input correction as long as it points in a direction of improving the robot's current motion under an implicit objective function. The proposed learning method is based on the cutting plane technique, which only utilizes the direction of a correction to update the objective function guess. We establish the theoretical results to show the convergence of the learned objective function towards the implicit one. We demonstrate the effectiveness of the method using numerical

simulations and two human-robot games. The results show the proposed method outperforms the state of the art, and that it enables a non-expert human user to teach a robot to learn an effective control objective function for satisfactory motion with few directional corrections.

APPENDIX

A. Proof of Lemma 1

The proof of Lemma 1 consists of two steps: first, we will derive the explicit form of the gradient quantity $\nabla J(\mathbf{u}_{0:T}^{\theta_k}, \theta^*)$, and second, we will show that (4) can be re-written as (1).

Consider the robot's current trajectory $\xi_{\theta_k} = \{\mathbf{x}_{0:T+1}^{\theta_k}, \mathbf{u}_{0:T}^{\theta_k}\}$, which satisfies the robot dynamics constraint in (1). For any $t = 0, 1, \dots, T$, define the infinitesimal increments $(\delta \mathbf{x}_t, \delta \mathbf{u}_t)$ at the state and input $(\mathbf{x}_t^{\theta_k}, \mathbf{u}_t^{\theta_k})$, respectively. By linearizing the dynamics (1) around $(\mathbf{x}_t^{\theta_k}, \mathbf{u}_t^{\theta_k})$, we have

$$\delta \mathbf{x}_{t+1} = \frac{\partial \mathbf{f}}{\partial \mathbf{x}_t^{\theta_k}} \delta \mathbf{x}_t + \frac{\partial \mathbf{f}}{\partial \mathbf{u}_t^{\theta_k}} \delta \mathbf{u}_t, \quad (50)$$

where $\frac{\partial \mathbf{f}}{\partial \mathbf{x}_t^{\theta_k}}$ and $\frac{\partial \mathbf{f}}{\partial \mathbf{u}_t^{\theta_k}}$ are the Jacobian matrices of \mathbf{f} with respect to \mathbf{x}_t and \mathbf{u}_t , respectively, evaluated at $(\mathbf{x}_t^{\theta_k}, \mathbf{u}_t^{\theta_k})$. By stacking (50) for all $t = 0, 1, \dots, T$ and also noting $\delta \mathbf{x}_0 = \mathbf{0}$ (because $\mathbf{x}_0^{\theta_k}$ is given), we have the following compact matrix from

$$-\mathbf{A}' \delta \mathbf{x}_{1:T+1} + \mathbf{B}' \delta \mathbf{u}_{0:T} = \mathbf{0}, \quad (51)$$

with $\delta \mathbf{x}_{1:T+1} = [\delta \mathbf{x}'_1, \dots, \delta \mathbf{x}'_{T+1}]'$, $\delta \mathbf{u}_{0:T} = [\delta \mathbf{u}'_1, \dots, \delta \mathbf{u}'_T]'$,

$$\mathbf{A} = \begin{bmatrix} \mathbf{F}_x & -\mathbf{V} \\ \mathbf{0} & I \end{bmatrix}, \quad \text{and} \quad \mathbf{B} = \begin{bmatrix} \mathbf{F}_u & \mathbf{0} \\ \mathbf{0} & \frac{\partial \mathbf{f}'}{\partial \mathbf{u}_T^{\theta_k}} \end{bmatrix}. \quad (52)$$

Here I is $n \times n$ identity matrix, \mathbf{F}_x and \mathbf{F}_u are defined in (9). Due to the increments $\delta \mathbf{x}_{1:T+1}$ and $\delta \mathbf{u}_{0:T}$, the change of the value of the cost $J(\mathbf{u}_{0:T}^{\theta_k}, \theta^*)$ in (2), denoted as $\delta J(\theta^*)$, can be written as

$$\delta J(\theta^*) = \mathbf{C}' \delta \mathbf{x}_{1:T+1} + \mathbf{D}' \delta \mathbf{u}_{0:T}, \quad (53)$$

with

$$\mathbf{C} = \begin{bmatrix} \Phi_x \theta^* \\ \frac{\partial h'}{\partial \mathbf{x}_{T+1}^{\theta_k}} \end{bmatrix} \quad \text{and} \quad \mathbf{D} = \begin{bmatrix} \Phi_u \theta^* \\ \frac{\partial \phi'}{\partial \mathbf{u}_T^{\theta_k}} \theta^* \end{bmatrix}, \quad (54)$$

with Φ_x and Φ_u are defined in (9). Considering \mathbf{A} is always invertible, we solve for $\delta \mathbf{x}_{1:T+1}$ from (51) and then submit it to (53), yielding

$$\begin{aligned}\delta J(\boldsymbol{\theta}^*) &= \mathbf{C}' \delta \mathbf{x}_{1:T+1} + \mathbf{D}' \delta \mathbf{u}_{0:T}, \\ &= \left(\mathbf{C}' (\mathbf{A}^{-1})' \mathbf{B}' + \mathbf{D}' \right) \delta \mathbf{u}_{0:T}.\end{aligned}\quad (55)$$

Thus, we have

$$\nabla J(\mathbf{u}_{0:T}^{\boldsymbol{\theta}_k}, \boldsymbol{\theta}^*) = \mathbf{B} \mathbf{A}^{-1} \mathbf{C} + \mathbf{D}.\quad (56)$$

The above (56) can be further written as

$$\begin{aligned}\nabla J(\mathbf{u}_{0:T}^{\boldsymbol{\theta}_k}, \boldsymbol{\theta}^*) &= \mathbf{B} \mathbf{A}^{-1} \mathbf{C} + \mathbf{D} \\ &= \begin{bmatrix} \mathbf{F}_u & \mathbf{0} \\ \mathbf{0} & \frac{\partial \mathbf{f}'}{\partial \mathbf{u}_T^{\boldsymbol{\theta}_k}} \end{bmatrix} \begin{bmatrix} \mathbf{F}_x & -\mathbf{V} \\ \mathbf{0} & \mathbf{I} \end{bmatrix}^{-1} \begin{bmatrix} \Phi_x \boldsymbol{\theta}^* \\ \frac{\partial h'}{\partial \mathbf{x}_{T+1}^{\boldsymbol{\theta}_k}} \end{bmatrix} \\ &\quad + \begin{bmatrix} \Phi_u \boldsymbol{\theta}^* \\ \frac{\partial \phi'}{\partial \mathbf{u}_T^{\boldsymbol{\theta}_k}} \boldsymbol{\theta}^* \end{bmatrix} \\ &= \begin{bmatrix} \mathbf{F}_u \mathbf{F}_x^{-1} \Phi_x \boldsymbol{\theta}^* + \Phi_u \boldsymbol{\theta}^* + \mathbf{F}_u \mathbf{F}_x^{-1} \mathbf{V} \frac{\partial h'}{\partial \mathbf{x}_{T+1}^{\boldsymbol{\theta}_k}} \\ \frac{\partial \phi'}{\partial \mathbf{u}_T^{\boldsymbol{\theta}_k}} \boldsymbol{\theta}^* + \frac{\partial f'}{\partial \mathbf{u}_T^{\boldsymbol{\theta}_k}} \frac{\partial h'}{\partial \mathbf{x}_{T+1}^{\boldsymbol{\theta}_k}} \end{bmatrix},\end{aligned}\quad (57)$$

where we have used Schur complement to compute the inverse of the block matrix \mathbf{A} . Using the definition in (8), (57) can be rewritten as

$$\begin{aligned}\nabla J(\mathbf{u}_{0:T}^{\boldsymbol{\theta}_k}, \boldsymbol{\theta}^*) &= \mathbf{H}_1(\mathbf{x}_{0:T+1}^{\boldsymbol{\theta}_k}, \mathbf{u}_{0:T}^{\boldsymbol{\theta}_k}) \boldsymbol{\theta}^* \\ &\quad + \mathbf{H}_2(\mathbf{x}_{0:T+1}^{\boldsymbol{\theta}_k}, \mathbf{u}_{0:T}^{\boldsymbol{\theta}_k}) \nabla h(\mathbf{x}_{T+1}^{\boldsymbol{\theta}_k}).\end{aligned}\quad (58)$$

Substituting (58) into the assumption (4) and also considering the definitions in (7), we obtain

$$\left\langle \nabla J(\mathbf{u}_{0:T}^{\boldsymbol{\theta}_k}, \boldsymbol{\theta}^*), \bar{\mathbf{a}}_k \right\rangle = \langle \mathbf{h}_k, \boldsymbol{\theta}^* \rangle + b_k < 0,\quad (59)$$

which leads to (6). This completes the proof. ■

B. Proof of Lemma 2

First, we prove (15). From Step 2 in the main algorithm, we know that the robot's current trajectory $\xi_{\boldsymbol{\theta}_k} = \{\mathbf{x}_{0:T+1}^{\boldsymbol{\theta}_k}, \mathbf{u}_{0:T}^{\boldsymbol{\theta}_k}\}$ is a result of minimizing the cost function $J(\boldsymbol{\theta}_k)$. This means that $\xi_{\boldsymbol{\theta}_k}$ must satisfy the optimality condition (i.e., first order condition) of the optimal control problem with the cost function $J(\boldsymbol{\theta}_k)$ in (2) and dynamics in (1). Following a similar derivation from (51) to (58) in the proof of Lemma 1, we can obtain

$$\begin{aligned}\mathbf{0} = \nabla J(\mathbf{u}_{0:T}^{\boldsymbol{\theta}_k}, \boldsymbol{\theta}_k) &= \mathbf{H}_1(\mathbf{x}_{0:T+1}^{\boldsymbol{\theta}_k}, \mathbf{u}_{0:T}^{\boldsymbol{\theta}_k}) \boldsymbol{\theta}_k + \\ &\quad \mathbf{H}_2(\mathbf{x}_{0:T+1}^{\boldsymbol{\theta}_k}, \mathbf{u}_{0:T}^{\boldsymbol{\theta}_k}) \nabla h(\mathbf{x}_{T+1}^{\boldsymbol{\theta}_k}).\end{aligned}\quad (60)$$

It is worth mentioning that the above optimality condition (60) is also derived in [5]. Thus,

$$0 = \left\langle \nabla J(\mathbf{u}_{0:T}^{\boldsymbol{\theta}_k}, \boldsymbol{\theta}_k), \bar{\mathbf{a}}_k \right\rangle\quad (61)$$

$$\begin{aligned}&= \left\langle \mathbf{H}_1(\mathbf{x}_{0:T+1}^{\boldsymbol{\theta}_k}, \mathbf{u}_{0:T}^{\boldsymbol{\theta}_k}) \boldsymbol{\theta}_k, \bar{\mathbf{a}}_k \right\rangle \\ &\quad + \left\langle \mathbf{H}_2(\mathbf{x}_{0:T+1}^{\boldsymbol{\theta}_k}, \mathbf{u}_{0:T}^{\boldsymbol{\theta}_k}) \nabla h(\mathbf{x}_{T+1}^{\boldsymbol{\theta}_k}), \bar{\mathbf{a}}_k \right\rangle\end{aligned}\quad (62)$$

$$= \langle \mathbf{h}_k, \boldsymbol{\theta}_k \rangle + b_k,\quad (63)$$

where the fourth line is due to the definition of hyperplane in (7). This completes the proof of (15).

Next, we prove (16). We use proof by induction. By the main algorithm, we know $\boldsymbol{\theta}^* \in \Omega_0$ for $k = 0$. Assume that $\boldsymbol{\theta}^* \in \Omega_{k-1}$ holds for the $(k-1)$ -th iteration. According to Step 3 in the main algorithm, we have the relationship

$$\Omega_k = \Omega_{k-1} \cap \{\boldsymbol{\theta} \in \Theta \mid \langle \mathbf{h}_k, \boldsymbol{\theta} \rangle + b_k < 0\}.\quad (64)$$

In order to prove $\boldsymbol{\theta}^* \in \Omega_k$ we only need to show that

$$\langle \mathbf{h}_k, \boldsymbol{\theta}^* \rangle + b_k < 0,\quad (65)$$

which is true according to (6) in Lemma 1. Thus, $\boldsymbol{\theta}^* \in \Omega_k$ also holds at the k th iteration. Thus, we conclude that (16) holds. This completes the proof of Lemma 2. ■

C. Other Choices of $\boldsymbol{\theta}_k$

For the search space $\Omega_k \subset \mathbb{R}^r$, we in this paper choose $\boldsymbol{\theta}_k$ as the center of Maximum Volume Ellipsoid (MVE) inscribe Ω_k . Other choices for $\boldsymbol{\theta}_k$ could be the center of gravity [30], the Chebyshev center [31], the analytic center [32], etc.

1) *Center of Gravity*: The center of gravity for a polytope Ω is defined as

$$\boldsymbol{\theta}_{\text{cg}} = \frac{\int_{\Omega} \boldsymbol{\theta} d\boldsymbol{\theta}}{\int_{\Omega} d\boldsymbol{\theta}}.\quad (66)$$

As proven by [33], the volume reduction rate using the center of gravity is

$$\frac{\text{Vol}(\Omega_{k+1})}{\text{Vol}(\Omega_k)} \leq 1 - \frac{1}{e} \approx 0.63,\quad (67)$$

which may lead to faster convergence than the rate $(1 - 1/r)$ using the center of MVE in Section IV when the parameter space is high dimensional (i.e., r large). However, for a polytope described by a set of linear inequalities, it requires much higher computational cost to obtain the center of gravity in (66) than solving the center of MVE inscribed in Ω_k [24].

2) *Chebyshev Center*: Chebyshev center is defined as the center of the largest Euclidean ball that lies inside the polytope Ω . The Chebyshev center for a polytope can be computed by solving a linear program [25], which is also efficient. But the Chebyshev center is not affinely invariant to the transformations of coordinates [24]. Therefore, a linear mapping of features may lead to an inconsistent weight vector estimation.

3) *Analytic Center*: Given a polytope $\Omega = \{\boldsymbol{\theta} \mid \langle \mathbf{h}_i, \boldsymbol{\theta} \rangle + b_i < 0, i = 1, \dots, m\}$, the analytic center is defined as

$$\boldsymbol{\theta}_{\text{ac}} = \min_{\boldsymbol{\theta}} - \sum_{i=1}^m \log(b_i - \mathbf{h}'_i \boldsymbol{\theta}).\quad (68)$$

As shown by [34], [35], using the analytic center achieves a good trade-off in terms of simplicity and practical performance, which however does not easily lead to the volume reduction analysis in Lemma 4 as choosing the center of MVE.

REFERENCES

- [1] H. Ravichandar, A. S. Polydoros, S. Chernova, and A. Billard, “Recent advances in robot learning from demonstration,” *Annual Review of Control, Robotics, and Autonomous Systems*, vol. 3, 2020.
- [2] M. Kuderer, S. Gulati, and W. Burgard, “Learning driving styles for autonomous vehicles from demonstration,” in *IEEE International Conference on Robotics and Automation*. IEEE, 2015, pp. 2641–2646.
- [3] P. Englert, N. A. Vien, and M. Toussaint, “Inverse kkt: Learning cost functions of manipulation tasks from demonstrations,” *The International Journal of Robotics Research*, vol. 36, no. 13-14, pp. 1474–1488, 2017.
- [4] W. Jin, T. D. Murphey, D. Kulić, N. Ezer, and S. Mou, “Learning from sparse demonstrations,” *arXiv preprint arXiv:2008.02159*, 2020.
- [5] W. Jin, D. Kulić, S. Mou, and S. Hirche, “Inverse optimal control with incomplete observations,” *arXiv preprint arXiv:1803.07696*, 2018.
- [6] A. Jain, S. Sharma, T. Joachims, and A. Saxena, “Learning preferences for manipulation tasks from online coercive feedback,” *The International Journal of Robotics Research*, vol. 34, no. 10, pp. 1296–1313, 2015.
- [7] P. Moylan and B. Anderson, “Nonlinear regulator theory and an inverse optimal control problem,” *IEEE Transactions on Automatic Control*, vol. 18, no. 5, pp. 460–465, 1973.
- [8] A.-S. Puydupin-Jamin, M. Johnson, and T. Bretl, “A convex approach to inverse optimal control and its application to modeling human locomotion,” in *International Conference on Robotics and Automation*, 2012, pp. 531–536.
- [9] W. Jin, D. Kulić, J. F.-S. Lin, S. Mou, and S. Hirche, “Inverse optimal control for multiphase cost functions,” *IEEE Transactions on Robotics*, vol. 35, no. 6, pp. 1387–1398, 2019.
- [10] A. Y. Ng, S. J. Russell *et al.*, “Algorithms for inverse reinforcement learning,” in *ICML*, vol. 1, 2000, p. 2.
- [11] B. D. Ziebart, A. L. Maas, J. A. Bagnell, and A. K. Dey, “Maximum entropy inverse reinforcement learning,” in *AAAI*, vol. 8, 2008, pp. 1433–1438.
- [12] N. D. Ratliff, J. A. Bagnell, and M. A. Zinkevich, “Maximum margin planning,” in *International Conference on Machine Learning*, 2006, pp. 729–736.
- [13] W. Jin, Z. Wang, Z. Yang, and S. Mou, “Pontryagin differentiable programming: An end-to-end learning and control framework,” *Advances in Neural Information Processing Systems*, vol. 33, 2020.
- [14] W. Jin, Z. Liang, and S. Mou, “Inverse optimal control from demonstration segments,” *arXiv preprint arXiv:2010.15034*, 2020.
- [15] C. Moro, G. Nejat, and A. Mihailidis, “Learning and personalizing socially assistive robot behaviors to aid with activities of daily living,” *ACM Transactions on Human-Robot Interaction*, vol. 7, no. 2, pp. 1–25, 2018.
- [16] A. Jain, B. Wojcik, T. Joachims, and A. Saxena, “Learning trajectory preferences for manipulators via iterative improvement,” in *Advances in neural information processing systems*, 2013, pp. 575–583.
- [17] A. Bajcsy, D. P. Losey, M. K. O’Malley, and A. D. Dragan, “Learning robot objectives from physical human interaction,” *Proceedings of Machine Learning Research*, vol. 78, pp. 217–226, 2017.
- [18] J. Y. Zhang and A. D. Dragan, “Learning from extrapolated corrections,” in *International Conference on Robotics and Automation*. IEEE, 2019, pp. 7034–7040.
- [19] D. P. Losey and M. K. O’Malley, “Including uncertainty when learning from human corrections,” *arXiv preprint arXiv:1806.02454*, 2018.
- [20] A. D. Dragan, K. Muelling, J. A. Bagnell, and S. S. Srinivasa, “Movement primitives via optimization,” in *2015 IEEE International Conference on Robotics and Automation (ICRA)*. IEEE, 2015, pp. 2339–2346.
- [21] R. Tedrake, “Underactuated robotics: Learning, planning, and control for efficient and agile machines course notes for mit 6.832,” *Working draft edition*, vol. 3, 2009.
- [22] W. Li and E. Todorov, “Iterative linear quadratic regulator design for nonlinear biological movement systems,” in *International Conference on Informatics in Control, Automation and Robotics*, 2004, pp. 222–229.
- [23] J. A. E. Andersson, J. Gillis, G. Horn, J. B. Rawlings, and M. Diehl, “CasADi – A software framework for nonlinear optimization and optimal control,” *Mathematical Programming Computation*, vol. 11, no. 1, pp. 1–36, 2019.
- [24] S. Boyd and L. Vandenberghe, “Localization and cutting-plane methods,” *From Stanford EE 364b lecture notes*, 2007.
- [25] S. Boyd, S. P. Boyd, and L. Vandenberghe, *Convex optimization*. Cambridge university press, 2004.
- [26] S. Diamond and S. Boyd, “CVXPY: A Python-embedded modeling language for convex optimization,” *Journal of Machine Learning Research*, vol. 17, no. 83, pp. 1–5, 2016.
- [27] S. P. Tarasov, “The method of inscribed ellipsoids,” in *Soviet Mathematics-Doklady*, vol. 37, no. 1, 1988, pp. 226–230.
- [28] J. B. Kuipers, *Quaternions and rotation sequences*. Princeton University Press, 1999, vol. 66.
- [29] T. Lee, M. Leok, and N. H. McClamroch, “Geometric tracking control of a quadrotor uav on $se(3)$,” in *IEEE Conference on Decision and Control*, 2010, pp. 5420–5425.
- [30] D. J. Newman, “Location of the maximum on unimodal surfaces,” *Journal of the ACM (JACM)*, vol. 12, no. 3, pp. 395–398, 1965.
- [31] J. Elzinga and T. G. Moore, “A central cutting plane algorithm for the convex programming problem,” *Mathematical Programming*, vol. 8, no. 1, pp. 134–145, 1975.
- [32] J.-L. Goffin and J.-P. Vial, “On the computation of weighted analytic centers and dual ellipsoids with the projective algorithm,” *Mathematical Programming*, vol. 60, no. 1-3, pp. 81–92, 1993.
- [33] B. Grünbaum *et al.*, “Partitions of mass-distributions and of convex bodies by hyperplanes,” *Pacific Journal of Mathematics*, vol. 10, no. 4, pp. 1257–1261, 1960.
- [34] D. S. Atkinson and P. M. Vaidya, “A cutting plane algorithm for convex programming that uses analytic centers,” *Mathematical Programming*, vol. 69, no. 1-3, pp. 1–43, 1995.
- [35] Y. Nesterov, “Cutting plane algorithms from analytic centers: efficiency estimates,” *Mathematical Programming*, vol. 69, no. 1, pp. 149–176, 1995.